The Astrophysical Journal, 572:861–879, 2002 June 20

THE CHEMICAL COMPOSITION AND AGE OF THE METAL-POOR HALO STAR BD +17°3248[1]

John J. Cowan,[2] Christopher Sneden,[3] Scott Burles,[4] Inese I. Ivans,[3] Timothy C. Beers,[5] James W. Truran,[6] James E. Lawler,[7] Francesca Primas,[8] George M. Fuller,[9] Bernd Pfeiffer,[10] and Karl-Ludwig Kratz[10]

Received 2001 November 19; accepted 2002 February 20

ABSTRACT

We have combined new high-resolution spectra obtained with the *Hubble Space Telescope* (*HST*) and ground-based facilities to make a comprehensive new abundance analysis of the metal-poor, halo star BD +17°3248. We have detected the third *r*-process peak elements osmium, platinum, and (for the first time in a metal-poor star) gold, elements whose abundances can only be reliably determined using *HST*. Our observations illustrate a pattern seen in other similar halo stars with the abundances of the heavier neutron capture elements, including the third *r*-process peak elements, consistent with a scaled solar system *r*-process distribution. The abundances of the lighter neutron capture elements, including germanium and silver, fall below that same scaled solar *r*-process curve, a result similar to that seen in the ultra–metal-poor star CS 22892-052. A single site with two regimes or sets of conditions, or perhaps two different sites for the lighter and heavier neutron capture elements, might explain the abundance pattern seen in this star. In addition, we have derived a reliable abundance for the radioactive element thorium. We tentatively identify U II at 3859 Å in the spectrum of BD +17°3248, which makes this the second detection of uranium in a very metal-poor halo star. Our combined observations cover the widest range in proton number (from germanium to uranium) thus far of neutron capture elements in metal-poor Galactic halo stars. Employing the thorium and uranium abundances in comparison with each other and with several stable elements, we determine an average cosmochronological age for BD +17°3248 of 13.8 ± 4 Gyr, consistent with that found for other similar metal-poor halo stars.

Subject headings: Galaxy: abundances — Galaxy: evolution — Galaxy: halo — nuclear reactions, nucleosynthesis, abundances — stars: abundances — stars: Population II

On-line material: color figures, machine-readable table

1. INTRODUCTION

The abundance distributions in Galactic halo stars indicate the extent of early Galactic nucleosynthesis and the nature of the earliest progenitor stars. Observations of neutron capture (*n*-capture) elements, in particular, provide a number of important clues about the early history, chemical evolution, and age of the Galaxy. There have been a number of observational and theoretical studies of the metal-poor halo stars, for example, that have established that the heavy *n*-capture elements were generally synthesized early in the history of the Galaxy by the *r*-process (Spite & Spite 1978; Truran 1981; Sneden & Parthasarathy 1983; Sneden & Pilachowski 1985; Krishnaswamy-Gilroy et al. 1988; Gratton & Sneden 1994; McWilliam et al. 1995a, 1995b; Cowan et al. 1995; Sneden et al. 1996, hereafter S96; Ryan, Norris, & Beers 1996). Evidence for substantial amounts of *s*-process *n*-capture products is confined mainly to very carbon-rich stars (see Aoki et al. 2001 and references therein).

Additional abundance studies of the halo stars have been employed to study the chemical evolution of the Galaxy. Of particular interest is the scatter in the mean level of the *n*-capture element to iron abundance ratios in stars of very low metallicity ([Fe/H] < −2.0).[11] First noted by Krishnaswamy-Gilroy et al. (1988) and confirmed by McWilliam et al. (1995a, 1995b) and Burris et al. (2000, hereafter B00), these observations suggest an early chemically inhomogeneous Galaxy. In contrast, surveys of Galactic disk stars with [Fe/H] > −1 (Edvardsson et al. 1993; Woolf, Tomkin, & Lambert 1995) show little scatter in *n*-capture bulk abundance levels. Other chemical evolution

[1] Based on observations made at three facilities: (1) the NASA/ESA *Hubble Space Telescope*, obtained at the Space Telescope Science Institute (STScI), which is operated by the Association of Universities for Research in Astronomy, Inc., under NASA contract NAS 5-26555; (2) the Keck I Telescope of the W. M. Keck Observatory, which is operated by the California Association for Research in Astronomy (CARA, Inc.) on behalf of the University of California and the California Institute of Technology; and (3) the H. J. Smith Telescope of McDonald Observatory, which is operated by the University of Texas at Austin.

[2] Department of Physics and Astronomy, Room 131 Nielsen Hall, University of Oklahoma, Norman, OK 73019; cowan@mail.nhn.ou.edu.

[3] Department of Astronomy and McDonald Observatory, University of Texas at Austin, Austin, TX 78712; chris@verdi.as.utexas.edu, iivans@astro.as.utexas.edu.

[4] Department of Physics, Massachusetts Institute of Technology, 77 Massachusetts Avenue, Room 6-113, Cambridge, MA 02139-4307; burles@mit.edu.

[5] Department of Physics and Astronomy, Michigan State University, East Lansing, MI 48824; beers@pa.msu.edu.

[6] Department of Astronomy and Astrophysics, Enrico Fermi Institute, University of Chicago, 933 East 56th Street, Chicago, IL 60637; truran@nova.uchicago.edu.

[7] Department of Physics, 2531 Sterling Hall, University of Wisconsin at Madison, Madison, WI 53706; jelawler@facstaff.wisc.edu.

[8] European Southern Observatory, Karl-Schwarzschild-Strasse 2, D-85748 Garching bei Muenchen, Germany; fprimas@eso.org.

[9] Department of Physics, Code 0354, 9500 Gilman Drive, University of California at San Diego, La Jolla, CA 92093-0319; gfuller@ucsd.edu.

[10] Institut für Kernchemie, Universität Mainz, Fritz-Strassmann-Weg 2, D-55099 Mainz, Germany; pfeiffer@mail.kernchemie.uni-mainz.de, klkratz@mail.kernchemie.uni-mainz.de.

[11] We adopt the usual spectroscopic notations that $[A/B] \equiv \log_{10}(N_A/N_B)_{star} - \log_{10}(N_A/N_B)_{\odot}$ and $\log \epsilon(A) \equiv \log_{10}(N_A/N_H) + 12.0$ for elements A and B. Furthermore, metallicity will be assumed here to be equivalent to the stellar [Fe/H] value.

studies have attempted to understand the changing nature of element production as a function of metallicity and time throughout the Galaxy's history (see Wheeler, Sneden, & Truran 1989 and references therein). Thus, while barium appears to be synthesized by the *r*-process at earliest times, this element is predominantly produced in solar system material by the *s*-process (see B00) in low- to intermediate-mass stars (Arlandini et al. 1999). Products of the *s*-process first appear in ordinary halo stars somewhere below a metallicity of -2, with the onset of the bulk of Galactic *s*-processing occurring near $[Fe/H] = -2$, presumably at an age equivalent to the stellar evolutionary lifetime of low- to intermediate-mass stars (B00).

The abundances of certain long-lived radioactive elements, such as thorium and uranium, act as nuclear chronometers and provide direct age determinations in ultra–metal-poor halo stars (those with $[Fe/H] \lesssim -2.5$, hereafter UMP stars). This technique has been used recently with Th (produced solely in the *r*-process), particularly with respect to the stable *r*-process element europium, in both halo field stars (S96; Cowan et al. 1997; Pfeiffer, Kratz, & Thielemann 1997; Cowan et al. 1999; Sneden et al. 2000a; Westin et al. 2000; Johnson & Bolte 2001) and globular cluster stars (Sneden et al. 2000b). To date, both nuclear chronometers Th and U have been detected in only one UMP star (Cayrel et al. 2001). Radioactive element age estimates depend sensitively on both theoretical nucleosynthesis predictions and accurate determinations of the stellar abundances of radioactive elements. Thus far the reliability of the technique, indicated by still large uncertainties in chronometric age estimates, has been limited by very few stellar detections of Th and/or U and correspondingly by few detections of the stable third *r*-process peak elements necessary to constrain theoretical predictions.

Despite surveys of large numbers of halo stars (Beers, Preston, & Shectman 1985, 1992), only a few UMP stars have been selected for extensive follow-up abundance studies. These include the now well-known UMP giant star CS 22892-052 (Sneden et al. 1994, 1996, 2000a; Cowan et al. 1995, 1997). While a great many elements have been detected in CS 22892-052 (second only to the Sun), abundance studies have been limited to ground-based observations. (Results from space-based observations of CS 22892-052 will be given in C. Sneden et al. 2002, in preparation.) This has prevented reliable abundance measures for the important third *r*-process peak elements Os and Pt, which have their strongest atomic transitions in the UV. These elements, along with lead, were first detected in a metal-poor halo star by Cowan et al. (1996). Uranium has only recently been found, for the first time, in the UMP star CS 31082-001 ($[Fe/H] = -2.9$; Cayrel et al. 2001). Westin et al. (2000) were able to obtain third *r*-process peak element abundances with the *Hubble Space Telescope* (*HST*), along with thorium, in the UMP ($[Fe/H] = -3.0$) star HD 115444. This was the first halo star with reliable abundance data on the heaviest stable elements and the radioactive element thorium. However, the other important nuclear chronometer, uranium, has not yet been detected in that star.

In this paper we present the results of an extensive series of observations regarding the metal-poor ($[Fe/H] = -2.1$) halo star BD $+17^\circ 3248$. A separate investigation of this star is of interest for three reasons. First, BD $+17^\circ 3248$ has relatively large ratios of *n*-capture elements to iron (see, e.g., B00), which made additional element detections likely. These very large relative *n*-capture overabundances in BD $+17^\circ 3248$ are similar to those in HD 115444, while being somewhat less than those in CS 22892-052 and CS 31082-001. Second, the overall [Fe/H] metallicity of BD $+17^\circ 3248$ is roughly a factor of 10 larger than those of the other very *n*-capture–rich stars. Third, BD $+17^\circ 3248$ is a warmer star than the others, by 400–500 K in $T_{\rm eff}$. Thus, BD $+17^\circ 3248$ was targeted as (perhaps) the most metal-rich of the very *n*-capture–rich halo stars, with somewhat different excitation/ionization atmospheric conditions, which might provide new abundance measurements and also might be suitable for a chronometric age estimate. In addition to the ground-based observations, we have obtained *HST* observations allowing a comprehensive analysis of the *n*-capture elements with the widest range in proton number so far in any halo star, from Ge to U. Our observations are presented in § 2, followed by a summary of the derivation of abundances in § 3. The significance of the derived *n*-capture abundances and application of radioactive chronometer elements to stellar age estimates are discussed in § 4, and conclusions are given in § 5.

2. OBSERVATIONS AND REDUCTIONS

UV data.—High-resolution spectra in the ultraviolet wavelength range 2410 Å $\leq \lambda \leq$ 3070 Å were obtained with the *HST* Space Telescope Imaging Spectrograph (STIS). The instrument was configured with echelle grating E230M centered at $\lambda = 2707$ Å, an entrance aperture of $0\farcs2 \times 0\farcs06$, and the near-UV MAMA detector, which combined to deliver a spectral resolving power of $R \equiv \lambda/\Delta\lambda \simeq 30,000$. Four individual spectra were gathered during the single *HST* visit for BD $+17^\circ 3248$, with a total integration time of 180 minutes. Standard *HST* pipeline reductions were employed to reduce the individual integrations to one-dimensional, flat-fielded, wavelength-calibrated spectra. We then operated on these spectra and combined them by employing the *HST* software tools of IRAF.[12] The final signal-to-noise ratio (S/N) of the spectrum was difficult to estimate because stellar absorption features overlap at these wavelengths; true spectral continuum windows are difficult to identify. From comparisons of synthetic and observed spectra we believe that S/N > 50 in the wavelength regions of interest for this study.

Near-UV data.—We employed the Keck I HIRES cross-dispersed echelle spectrograph (Vogt et al. 1994) to acquire high-resolution spectra in the wavelength interval 3150 Å $\leq \lambda \leq$ 4600 Å. The spectral coverage was complete throughout this range. The resolving power of the fully reduced spectrum was $R \simeq 45,000$. Estimation of the S/N was not easy at the shortest wavelengths, but certainly the S/N decreased blueward, from ~300 at $\lambda \sim 4500$ Å to ~30 at $\lambda \sim 3200$ Å, as a result of the combined effects of decreasing stellar flux and CCD response in the UV. We also obtained standard auxiliary spectra of a tungsten lamp for flat-fielding the spectrum and a Th-Ar lamp for wavelength calibration. We performed a full echelle extraction, including flat-field and bias correction, cosmic-ray rejection, sky

[12] IRAF is distributed by the National Optical Astronomy Observatory, which is operated by the Association of Universities for Research in Astronomy, Inc., under cooperative agreement with the National Science Foundation.

subtraction, and wavelength and flux calibration, utilizing the software package MAKEE (e.g., Barlow & Sargent 1997).

Longer wavelength data.—We obtained a high-resolution spectrum spanning from the violet to the near-IR with the McDonald Observatory 2.7 m H. J. Smith telescope and the "2d-coudé" cross-dispersed echelle spectrograph (Tull et al. 1995). In addition to tungsten and Th-Ar calibration spectra, we also acquired a spectrum of the hot, rapidly rotating star ζ Aql to assist in cancellation of telluric (O_2 and H_2O) absorption features in the yellow–red wavelength region. With the spectrograph configured with a 1.″2 entrance slit and a Tektronix 2048×2048 CCD detector, the 2 pixel spectral resolving power was $R \simeq 60,000$. The useful wavelength range was 3750 Å $\leq \lambda \leq$ 9500 Å. The spectrum was continuous for $\lambda < 5900$ Å, but the increasing free spectral range of orders longward of this wavelength created some gaps in spectral coverage. The S/N value of the BD +17°3248 spectrum after completion of the reduction procedures was greater than 250 for $\lambda > 5500$ Å and declined steadily to levels of ~130 at $\lambda \sim 4200$ Å. Initial processing of the raw spectra (bias subtraction and frame trimming, scattered light removal, cosmic-ray excision, flat-fielding, spectral order extraction, and wavelength calibration) was accomplished with standard IRAF echelle reduction tasks.

Processing the spectra.—The final reduction tasks discussed here were accomplished with the specialized spectrum manipulation software package SPECTRE (Fitzpatrick & Sneden 1987). For all stellar data we eliminated individual bad data points and then normalized the spectral continua by fitting third-order spline functions to sets of interactively chosen continuum points. Additionally, all of the STIS spectral orders were smoothed via convolution with a 2 pixel FWHM Gaussian function. Equivalent widths (EWs) of selected lines were measured by either fitting Gaussian profiles to the spectral lines or direct (Simpson's rule) integrations over the line profiles; sometimes both methods were employed for lines that were partially blended or had asymmetric line shapes. The EWs of atomic species of elements with $Z \leq 30$ were needed to determine a new model atmosphere for BD +17°3248 and to confirm that this star has a typical Population II abundance mix, and EWs of many species with $Z > 30$ were employed in the *n*-capture abundance analysis. The line lists for these tasks are described in § 3.

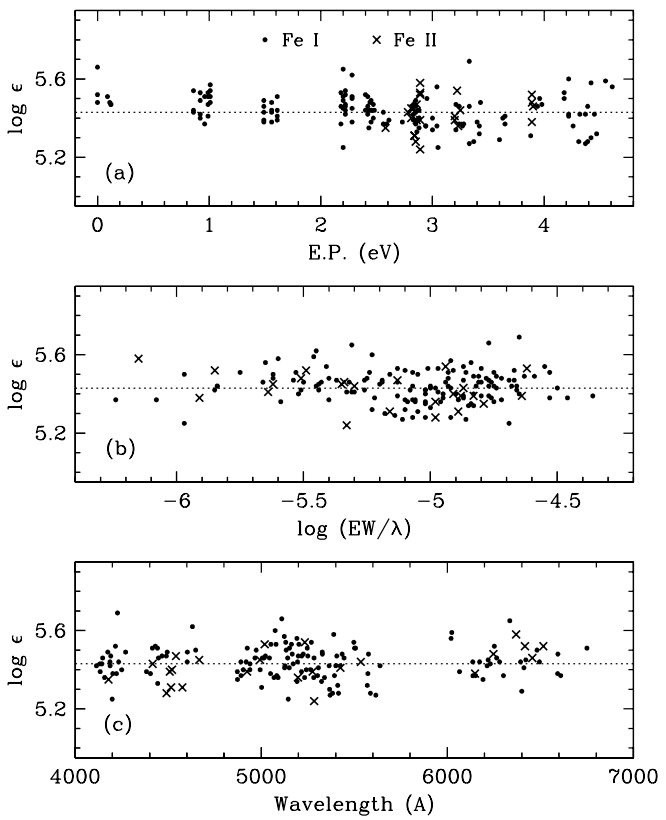

FIG. 1.—Abundances of Fe I and Fe II lines in BD +17°3248 as functions of (*a*) excitation potential, (*b*) logarithm of the reduced equivalent width, and (*c*) wavelength, using the adopted model atmosphere.

3. ABUNDANCE ANALYSIS

3.1. *Derivation of the Model Atmosphere*

We first determined new model atmosphere parameters $T_{\rm eff}$, $\log g$, [M/H], and v_t for BD +17°3248 using the EW data. This was accomplished in a standard LTE analysis that sought to derive (1) $T_{\rm eff}$, from minimizing the line-to-line abundance differences with excitation potential EP (mainly for Fe I); (2) v_t, from minimizing the line-to-line abundance differences with EW; (3) $\log g$, from forcing reasonable agreement between the neutral and ionized species of Ti and Fe; and (4) [M/H], from the approximate mean abundance level of the Fe peak elements and the α-capture elements Mg, Si, and Ca. We employed the line lists of Westin et al. (2000) for these and all other species with $Z \leq 30$. Trial model stellar atmospheres were generated from the Kurucz (1995)[13] grid with interpolation software kindly provided by A. McWilliam (2001, private communication). Abundances were computed for each line with the current version of the line analysis code of Sneden (1973), iterating various atmosphere parameter combinations until the best overall model was achieved.

In Figure 1 the correlations of Fe I and Fe II lines with EP, reduced equivalent width $\log(\mathrm{EW}/\lambda)$, and wavelength are shown for the adopted model: $(T_{\rm eff}, \log g, [\mathrm{M/H}], v_t) = (5200\ \mathrm{K},\ 1.80,\ -2.0,\ 1.9\ \mathrm{km\ s^{-1}})$. Within the scatter of individual line measurements ($\sigma = 0.08$ for Fe I and 0.09 for Fe II) there are no obvious trends in the Fe abundances. Additionally, the same model atmosphere choice yields no anomalous trends in the line-to-line abundances of any other species. Thus, the model atmosphere is internally well determined.

For external comparisons, note first that our model atmosphere parameters are in good agreement with those from all but one of the few prior spectroscopic investigations of BD +17°3248. Luck & Bond (1981) provided an initial set of parameters from photographic coudé spectra: (5000 K, 1.80, −2.0, 3.0 km s^{-1}). B00 derived abundances for a few *n*-capture elements in this star but adopted the Pilachowski, Sneden, & Kraft (1996) model atmosphere parameters: (5250 K, 2.30, −1.80, 1.5 km s^{-1}). Those values were determined from combined photometric and (very limited) spectroscopic information. Recently, Johnson & Bolte (2001)

[13] See http://cfaku5.harvard.edu.

have obtained their own Keck I HIRES spectrum of BD +17°3248, and their model atmosphere, derived in the same manner as we have done, has parameters essentially identical to ours: (5200 K, 1.80, −1.95, 1.90 km s^{-1}). The only substantial differences are seen with the investigation of Klochkova, Ermakov, & Panchuk (1999), who suggest that BD +17°3248 is a much hotter star, with corresponding increases in gravity and metallicity: (5590 K, 2.4, −1.15, 1.1 km s^{-1}). However, these parameters seem to be incompatible with the other high-resolution spectroscopic studies and with photometric data for this star that will be considered next.

In comparing our model atmosphere parameters with ones derived from photometric indicators, caution should be employed because reddening estimates for BD +17°3248 are larger than for many halo stars [$E(B-V) = 0.06$, Bond 1980; $E(b-y) = 0.040$, translating to $E(B-V) = 0.055$, Anthony-Twarog & Twarog 1994; B. J. Anthony-Twarog & B. A. Twarog 2001, private communication]. Such reddening can introduce substantial uncertainties in photometric temperature and gravity estimates.

Extant broadband photometry includes *UBV* measures $V = 9.37$ and $B-V = 0.66$ (Carney 1983) and IR measures $J = 7.815$, $H = 7.400$, and $K = 7.310$ (Alonso, Arribas, & Martinez-Roger 1998). The $V-K$ color is often thought to be the best broadband photometric temperature indicator. Alonso, Arribas, & Martinez-Roger (1999, 2001) recommend formulae for converting $V-K$ values and [Fe/H] estimates to $T_{\rm eff}$, but there are two complications for BD +17°3248. First, this star has a $V-K$ in the overlap region between two different Alonso et al. (1999, 2001) formulae for $T_{{\rm eff},V-K}$. Second, BD +17°3248 has been classified as a red horizontal branch (RHB) star (Bond 1980; Pilachowski et al. 1996; Alonso et al. 1998). Thus, since the Alonso et al. (1999, 2001) formulae strictly apply to first-ascent true red giant branch (RGB) stars, application of them to BD +17°3248 may be questionable. Remembering these caveats, adopting [Fe/H] = −2.1 in the $T_{\rm eff}$ calculations, and (for the moment) assuming no interstellar reddening, the observed $V-K = 2.06$ yields $T_{{\rm eff},V-K} = 4985$ and 5025 K (rounding the value to the nearest 5 K) using equations (8) and (9), respectively, from Table 2 of Alonso et al. (1999, 2001). However, if BD +17°3248 is reddened according to the Bond (1980) and Anthony-Twarog & Twarog (1994) estimates, and if the intrinsic $V-K$ color may be estimated as $(V-K)_{\rm int} \approx (V-K)_0 - A_V \approx (V-K) - 3E(B-V) = 1.88$, then $T_{{\rm eff},V-K} = 5280$ and 5260 K from equations (8) and (9), respectively, of Alonso et al. (1999, 2001). Thus, the spectroscopic and photometric temperature estimates for BD +17°3248 agree well if $E(B-V) \approx 0.06$.

The *JHK* photometry of BD +17°3248 also can be employed to estimate $T_{\rm eff}$ without reference to shorter wavelength photometry, thus avoiding reddening questions. From the Alonso et al. (1999) equation (10), the observed $J-H = 0.415$ yields $T_{{\rm eff},J-H} = 5080$ K, and from equation (11) the observed $J-K$ yields $T_{{\rm eff},J-K} = 5010$ K (this value is independent of assumed metallicity). Therefore, the total range in broadband photometric temperature estimates is about 300 K, which happily encompasses the spectroscopic value. The photometric $T_{\rm eff}$ range is unlikely to be narrowed further as a result of the RHB status and the uncertain reddening of BD +17°3248.

Photometry and a distance estimate for BD +17°3248 can provide an "evolutionary" gravity via the standard formula

$$\log g_{\rm evol} = -12.50 + 0.4(M_V + {\rm BC}) + \log M + 4 \log T_{\rm eff} ,$$

where BC is the bolometric correction and M is the stellar mass. Using the spectroscopic $T_{\rm eff} = 5200$ K, equation (18) of Alonso et al. (1999, 2001) gives BC = −0.21, and this value is consistent with other estimates (e.g., Bell & Gustafsson 1978). The mass of BD +17°3248 should lie between that of a typical main-sequence turnoff Population II star, 0.85 $M_\odot$, and that of an HB star, 0.55 $M_\odot$. A *Hipparcos* parallax (Perryman et al. 1997) exists, albeit with a large uncertainty: $\pi = 3.67 \pm 1.50$ mas. This parallax and the V magnitude correspond to $M_V = 2.16^{+0.74}_{-1.14}$, placing the star on the subgiant branch. This in turn implies with the above formula that $2.4 \lesssim \log g \lesssim 3.4$, the entire range of possible values being much larger than we determined from the BD +17°3248 spectrum (see also Fig. 9 of Carbon et al. 1982). This higher gravity is at odds with the highly evolved position of BD +17°3248 in the Strömgren c_1 versus $b-y$ diagram (Fig. 5 of Bond 1980), which has been shown to be a robust indicator of evolutionary state for cool metal-poor stars (Pilachowski, Sneden, & Booth 1993; Gratton et al. 2000). The *Hipparcos* parallax probably should be disregarded for this star.

Bond (1980) estimated $M_V \approx -0.2$ for BD +17°3248, and if this star belongs to the RHB, then $M = 0.55$ $M_\odot$. These values and an assumption of $T_{\rm eff} = 5200$ K lead to $\log g_{\rm evol} \approx 1.8$, in excellent agreement with the spectroscopic value. If we instead assume a temperature at the high end of the estimates, $T_{\rm eff} = 5600$ K (Klochkova et al. 1999), a higher absolute magnitude estimate, $M_V \approx 0.65$ (Anthony-Twarog & Twarog 1994; B. J. Anthony-Twarog & B. A. Twarog 2001, private communication), and a main-sequence mass of $M = 0.85$ $M_\odot$, then $\log g \approx 2.6$. A similar extension of parameters in the opposite direction yields $\log g \approx 1.6$. This exercise, just as in the comparison of spectroscopic and photometric temperature estimates, confirms that the spectroscopic gravity is not far from the evolutionary value, but uncertainties in (especially) the absolute magnitude of BD +17°3248 preclude more definitive statements.

Our metallicity value can also be compared to earlier literature estimates. From *uvby* photometry, Bond (1980) originally derived $[{\rm Fe/H}]_{uvby} = -2.0$, and more recently Anthony-Twarog & Twarog (1998) have suggested $[{\rm Fe/H}]_{uvby} = -2.16$. Beers & Sommer-Larsen (1995) estimated metallicities for a large sample of halo stars from a variety of photometric and low-resolution spectroscopic surveys in the literature and gave [Fe/H] = −2.0 for BD +17°3248. Beers et al. (1999) used broadband photometry, Ca II K line EWs, and medium-resolution spectra of a large sample of metal-poor stars to provide a uniform [Fe/H] scale over three decades of stellar metallicity, and in their system they derived $[{\rm Fe/H}]_{\rm K\ line} = -2.07 \pm 0.13$ for BD +17°3248. Photometry on the DDO system, using the calibration of Clariá et al. (1994) and the observations of Hartkopf & Yoss (1982), yields $[{\rm Fe/H}]_{\rm DDO} = -2.21 \pm 0.14$. The derived [Fe/H] values from the previous high-resolution spectroscopic analyses (neglecting the discordant value of Klochkova et al. 1999) are −2.04 (Luck & Bond 1981), −2.02 (Pilachowski et al. 1996), and −2.11 (Johnson & Bolte 2001). In short, the metallicity of BD +17°3248 appears to be well established, as the literature photometric

and spectroscopic estimates are in good accord with our derived [Fe/H] = −2.09. Considering all the available spectroscopic and photometric information for BD +17°3248, we suggest that the model atmospheric parameters for this star are well determined at $(T_{\rm eff}, \log g, [{\rm M/H}], v_t) = (5200 \pm 150\ {\rm K}, 1.80 \pm 0.3, -2.0 \pm 0.2, 1.9 \pm 0.2\ {\rm km\ s^{-1}})$.

3.2. *Abundances of Elements with $Z \leq 30$*

With our final spectroscopically determined model atmosphere for BD +17°3248 we then computed the abundances of almost all of the non–*n*-capture elements using the measured EWs. Abundances of light elements Li, C, N, and O were derived from matching synthetic spectra to the observed features of the Li I λ6708 resonance doublet, the CH $A\ ^2\Delta$–$X\ ^2\Pi$ G band from 4358 to 4372 Å, the NH $A\ ^3\Pi_i$–$X\ ^3\Sigma^-$ 0–0 and 1–1 bands from 3355 to 3375 Å, the CN $B\ ^2\Sigma^+$–$X\ ^2\Sigma^+$ 0–0 and 1–1 bands from 3869 to 3884 Å, and the [O I] λ6300 line. For details about the construction of the line lists employed in these computations the reader is referred to Sneden et al. (1991b), Westin et al. (2000), and Gratton et al. (2000). The Li I feature is extremely weak [EW ≤ 1.5 mÅ or log(EW/λ) ≤ −6.6], and our detection of it in BD +17°3248 must be considered tentative. The primary N abundance indicator is NH, since the CN absorption even at the 0–0 band head at 3883 Å is no more than 10% of the continuum, and the N abundance derived from CN depends directly on the assumed abundance of C.

The derived abundances of $Z \leq 30$ elements are given in Table 1 and graphically displayed in Figure 2. Elements whose derived abundances are based on only one or two lines (Al, V, Co, Cu, and Zn) clearly should be treated with caution. Here we will elaborate on a few of the abundances.

First, note that the Na abundance has been derived from the Na I λλ5685 and 8190 doublets. Use of the Na D resonance lines would yield about a factor of 4 larger abundance than that determined from the higher excitation lines. This apparent anomaly is similar to that found in RHB stars of similar-metallicity globular clusters M92 and M15 (Sneden et al. 1997; Sneden, Pilachowski, & Kraft 2000c). In these clusters, the D lines and the λ5680 doublets give similar abundance values in true first-ascent RGB, but not RHB, stars. This lends inferential support to the suggested RHB status of BD +17°3248. The spectra of RHB stars in M92 and M15 are most easily distinguished from those of the RGB stars by the presence of Hα emission (Sneden et al. 2000c; Pilachowski & Sneden 1999), but unfortunately this feature fell in one of the gaps of our McDonald spectral order coverage. Observations taken in 1983 as part of the Hα survey of metal-poor field giants by Smith & Dupree (1988) do not show Hα core emission, but this star was not included in their more recent survey (Dupree & Smith 1995). R. Cayrel (2001, private communication) finds no Hα anomaly in their new VLT spectrum of BD +17°3248. Further comparison of chromospheric features in this star with those in RGB stars of comparable metallicity and absolute magnitude would be welcome.

Second, the very low Al abundance, determined from only the Al I λ3961 resonance line, may not represent the true Al content of BD +17°3248. It is well known that the higher excitation lines in the red spectral region yield substantially larger Al abundances than those derived from the resonance lines. A good discussion of this problem and references to previous work are given in Ryan et al. (1996). Unfortunately, none of the lines of the Al I λλ6697 or 8773 doublets could be detected in our spectra of BD +17°3248, and estimated EW upper limits of ≈2 mÅ translated to an Al upper limit ≈1.5 dex larger than the abundance derived

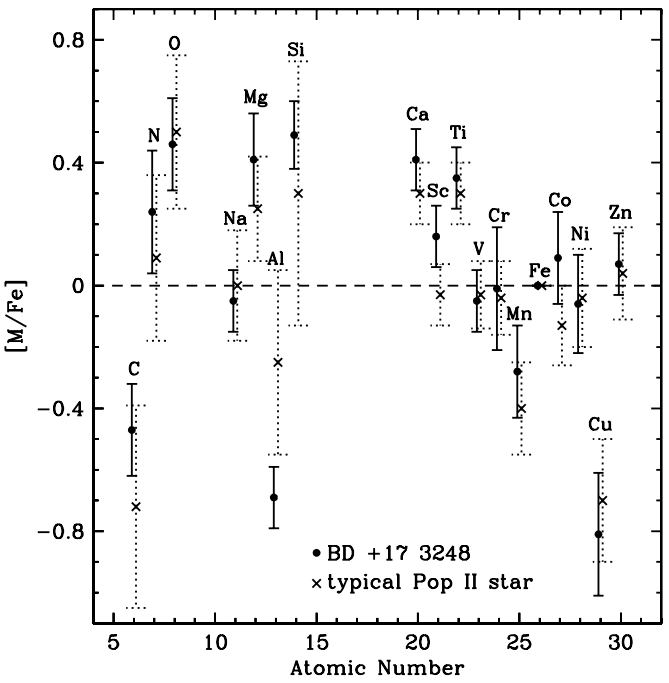

FIG. 2.—Abundance ratios for elements with $Z \leq 30$ derived in this analysis of BD +17°3248 and mean ratios for typical Population II stars. Most of the Population II star mean abundance ratios are taken from Fig. 4 (the points for metallicity [Fe/H] = −2.4) of Cayrel's (1996) review paper. The mean ratios for C and N come from Kraft et al. (1982), the value for V is from Gratton & Sneden (1991), and those for Cu and Zn are from Sneden et al. (1991b). The error bar plotted for a BD +17°3248 abundance is the larger of 0.10 dex or the sample standard deviation from Table 1.

TABLE 1
ABUNDANCES OF LIGHTER ELEMENTS FOR BD +17°3248

Species	Z	$\log \epsilon$	σ	Number	[M/Fe]
Li I	3	≲0.2	...	1	...
CH	6	6.00	(0.15)	...	−0.47
NH	7	6.20	(0.20)	...	0.24
[O I]	8	7.30	(0.15)	1	0.46
Na I	11	4.19	0.04	4	−0.05
Mg I	12	5.90	0.10	3	0.41
Al I	13	3.69	(0.15)	1	−0.69
Si I	14	5.95	0.11	6	0.49
Ca I	20	4.68	0.06	19	0.41
Sc II	21	1.17	0.05	5	0.16
Ti I	22	3.23	0.09	13	0.33
Ti II	22	3.27	0.13	19	0.37
V I	23	1.86	0.01	2	−0.05
Cr I	24	3.45	0.06	5	−0.13
Cr II	24	3.69	0.09	4	0.11
Mn I	25	3.02	0.15	2	−0.28
Fe I	26	5.44	0.08	139	0.01
Fe II	26	5.42	0.09	24	−0.01
Co I	27	2.92	(0.15)	1	0.09
Ni I	28	4.10	0.16	4	−0.06
Cu I	29	1.31	(0.15)	1	−0.81
Zn I	30	2.58	(0.15)	1	0.07

from the λ3961 resonance line. The upper limit from the red lines is not helpful, and so the Al abundance of BD +17°3248 must remain ill-determined at present, although following the lead of Ryan et al. (1996) we suspect that the true abundance may be larger than we have determined from the resonance line.

Finally, note that the abundance of O in metal-poor stars is a controversial subject at present. Analyses of [O I] and OH IR vibration-rotation lines yield [O/Fe] $\simeq 0.4$ independent of [Fe/H] over the entire halo metallicity range (e.g., Gratton et al. 2000 and references therein; Balachandran & Carney 1996; Meléndez, Barbuy, & Spite 2001), but O I high-excitation triplet lines and OH near-UV electronic band lines yield linearly increasing [O/Fe] values with decreasing metallicity, reaching [O/Fe] ~ 1 at [Fe/H] ~ -3 (Israelian, Gracía Lopez, & Rebolo 1998; Boesgaard et al. 1999). In BD +17°3248 the [O I] λ6300 line and all λ7770 triplet lines were detected, and our analysis reproduced the clash between these two O abundance indicators: from the forbidden line we derived [O/Fe] = 0.46, and from the triplet lines we found [O/Fe] = 0.72. In Table 1 we quote the abundance derived from the [O I] line because that is the usual O abundance indicator for halo giant stars. The analysis of BD +17°3248 sheds no additional light on the general O abundance problem of metal-poor stars, and a full examination of this issue is beyond the scope of our study.

In order to place the $Z < 30$ elemental abundances of BD +17°3248 in context with general Population II abundance trends, we add to Figure 2 estimates of mean [M/Fe] ratios for field stars of similar metallicity. For most elements, these overall abundance means were taken from the points representing stars of [Fe/H] ≈ -2.4 in Figure 4 of Cayrel (1996). Among elements not considered in Cayrel's review, the source for the mean V abundance is Gratton & Sneden (1991), and for Cu and Zn it is Sneden, Gratton, & Crocker (1991a). The abundances of the volatile elements Li, C, and N change with evolutionary state. Therefore, for the Population II abundance trends of C and N we used mean values from the Kraft et al. (1982) survey of C and N in halo field giant stars with metallicities more similar on average to that of BD +17°3248. These means were computed considering only those Kraft et al. (1982) stars that are thought to be chemically evolved, by adopting a luminosity limit of $M_V < -0.5$. These means are not very different from more recent results for evolved stars in the higher metallicity domain $-1 >$ [Fe/H] > -2 (Gratton et al. 2000). Abundances of Li are not pictured in Figure 2 because its origin in the halo is due to initial big bang nucleosynthesis and it is destroyed in normal stellar evolution; thus, values of [Li/Fe] are not meaningful. However, our abundance $\log \epsilon(\mathrm{Li}) \lesssim 0.2$ is in accord with the upper limit for field RHB stars of the Gratton et al. (2000) survey [$\log \epsilon(\mathrm{Li}) < 0.2$].

The comparison of abundance sets in Figure 2 indicates that the abundances of elements with $Z \leq 30$ in BD +17°3248 conform to the usual Population II abundance pattern in this metallicity domain: elevated abundances of α-capture elements Mg, Si, Ca, and Ti; large deficiencies of Al and Mn; and relatively normal abundances of most of the Fe peak elements. Any deviations from this pattern are significantly less than the uncertainties in the derived BD +17°3248 abundances.

3.3. *Abundances of the Neutron Capture Elements*

Abundances of 26 *n*-capture elements and a significant upper limit for a 27th one were determined from EW matches for unblended single lines and from synthetic spectrum computations for blended lines and/or lines with significant hyperfine and/or isotopic splitting. The *n*-capture abundance analysis generally followed the ones described by S96 and Sneden et al. (2000a) for CS 22892-052, Westin et al. (2000) for HD 115444, and Sneden et al. (1998) for UV spectral region *n*-capture transitions in HD 115444 and HD 126238. We began with the line lists that were developed for those papers. However, in the past several years significant improvements have been made to the atomic line parameters of several *n*-capture elements, particularly for some singly ionized species of rare earth elements. Additionally, the brief Sneden et al. (2000a) paper on CS 22892-052 did not discuss transition probability choices for the new *n*-capture elements reported in that study. Finally, the combination of higher temperature and metallicity of BD +17°3248 compared to CS 22892-052 and HD 115444 sometimes reveals different sets of spectral features of these species for analysis than were best for the other two stars. Therefore, we reconsidered the abundance determinations for all *n*-capture elements, and in the Appendix we comment on those species that have had significant updates in line list parameters or are otherwise deserving of some detailed discussion.

The construction of synthetic spectrum line lists is described in S96 and Sneden et al. (1998). Briefly, we culled the lists of atomic lines from the Kurucz (1995) database, retaining H I Balmer lines and those atomic lines of neutral and singly ionized species whose excitation potentials were less than 5 eV. Trial synthetic spectrum computations showed that only transitions meeting these criteria would produce measurable absorption in our spectra of cool, metal-poor stars. We supplemented these lines with a few that are identified in the Moore, Minnaert, & Houtgast (1966) solar atlas but are missing from the Kurucz database. The relevant molecular lines are in almost all cases the hydrides CH, NH, and OH. Again starting from the Kurucz lists, we kept lines of these molecules that had EP $\lesssim 1.5$, since transitions beginning at higher excitation levels of these easily dissociated molecules are generally bound-free transitions that proved to be undetectable in our observed spectra. To account for a few absorptions in the spectra that have no obvious atomic and molecular identification, we arbitrarily assumed that they were Fe I lines with EP = 3.5 eV.

We refined these line lists by matching synthetic and observed spectra of the solar photosphere for spectral regions covered by our ground-based Keck and McDonald spectra. The solar spectrum was an electronic copy of the Kurucz et al. (1984) solar flux atlas,[14] and the chosen solar model atmosphere was that of Holweger & Müller (1974). The transition probabilities of the *n*-capture element transitions were taken from the atomic physics literature without change (see the Appendix), but the *gf*-values of the surrounding atomic spectral features were altered to match the solar spectrum. Except for the syntheses described in § 3.2 for the determination of CNO abundances, the molecular lines were treated simply as contaminants. Relative line

[14] See URL given in footnote 13.

strengths of different rotational lines of molecular electronic bands can be determined to better precision than overall band strengths. Therefore, for an individual synthesis we varied the absorptions of a given molecule as a set by simply varying the assumed abundance of C, N, or O.

However, the solar spectrum in the UV is dominated by overlapping saturated lines, and there is no routinely accessible electronic solar spectrum below $\lambda \lesssim 3000$ Å. Thus, following the procedure of Sneden et al. (1998), we chose the bright UMP giant HD 122563 (4500 K, 1.30, −2.7, 2.5 km s^{-1}; Westin et al. 2000) as the template star for spectral regions covered by our *HST*/STIS spectrum. This choice took advantage of the underabundance of *n*-capture elements with $Z \geq 56$ in HD 122563, e.g., [Eu/Fe] $\simeq -0.4$ (Westin et al. 2000 and references therein). This deficiency results in no detectable absorptions due to third *n*-capture element transitions either in the *HST*/GHRS spectra of Sneden et al. (1998) or in our new *HST*/STIS spectrum of this star. Thus, HD 122563 provides an excellent template spectrum to assist in modeling the strengths of other atomic and molecular contaminants to the *n*-capture transitions of interest.

After iterating the synthetic spectrum line lists to produce reasonable agreement with the solar or HD 122563 spectrum, we then applied them to matching the spectrum of BD +17°3248. The resulting line-by-line BD +17°3248 *n*-capture abundances are presented in Table 2. For unblended lines of *n*-capture species that are unaffected by isotopic or hyperfine structure problems, the fourth column of Table 2 gives the EW of the line that was used in the abundance derivation. For the more complex features requiring synthetic spectrum computations, the notation "Syn" is given in the fourth column.

The mean $\log \epsilon$ and [X/Fe] values for the *n*-capture elements in BD +17°3248 are given in Table 3, along with sample standard deviations σ and the number of lines analyzed. The [X/Fe] ratios were computed by assuming that [Fe/H] = −2.09 and adopting the recommended solar abundances $\log \epsilon_{\odot}$ of Grevesse & Sauval (1998), which also are listed in Table 3. For a few elements, recent solar photospheric abundance studies (e.g., Lawler et al. 2001b for Tb II) derive abundances that ultimately may supersede the solar numbers in Table 3. However, here we are using the [X/Fe] ratios only as general guides to *n*-capture element enhancements, so for simplicity we will employ only the Grevesse & Sauval (1998) solar abundances.

For some elements with only a few detected lines, nominal σ values turned out fortuitously to be very small. However, the line-to-line scatters for elements possessing many transitions suggest that more realistic minimum measurement and internal analysis uncertainties for single lines are ∼0.05 dex. Therefore, we have adopted more conservative scatter values for Table 3 and figures that use the data of this table: for a species with three or more lines, σ equals the greater of the measured value or 0.05 dex; for a species with two lines, the greater of the measured value or 0.10 dex; and for a species with only one line, 0.15 dex. The only exception to this is for U, which we consider below.

Two other recent spectroscopic studies have reported *n*-capture abundances for BD +17°3248. Johnson & Bolte (2001) derived abundances for seven rare earth elements, and the mean abundance difference is $\langle \Delta[n\text{-capture/Fe}] \rangle \equiv [n\text{-capture/Fe}]_{\rm JB01} - [n\text{-capture/Fe}]_{\rm us} = 0.02 \pm 0.04$ ($\sigma = 0.10$). This is excellent agreement con-

TABLE 2

NEUTRON CAPTURE LINES IN BD +17°3248

λ (Å)	EP (eV)	log *gf*	EW (mÅ)	log ϵ
Ge I, $Z = 32$				
3039.07	0.88	−0.04	Syn	0.60
Sr I, $Z = 38$				
4607.33	0.00	0.28	Syn	0.90
Sr II, $Z = 38$				
4077.71	0.00	0.17	Syn	1.05
4215.52	0.00	−0.17	Syn	1.15
Y II, $Z = 39$				
3549.01	0.13	−0.28	59.0	0.09
3600.74	0.18	0.28	74.0	−0.02
3611.04	0.13	0.01	67.5	0.01
3747.55	0.10	−0.91	35.0	0.03
3774.33	0.13	0.22	85.0	0.09
3788.70	0.10	−0.07	76.5	0.10
3950.36	0.10	−0.49	59.0	0.05
4398.01	0.13	−1.00	36.5	0.07
5087.43	1.08	−0.17	25.5	0.00
5200.42	0.99	−0.57	14.0	−0.03
5205.73	1.03	−0.34	23.0	0.04
Zr II, $Z = 40$				
3036.39	0.56	−0.42	Syn	0.60
3036.51	0.53	−0.60	Syn	0.60
3054.44	0.71	−1.20	Syn	0.85
3060.11	0.04	−1.37	Syn	0.70
3061.33	0.09	−1.38	Syn	0.50
3424.82	0.04	−1.31	23.0	0.69
3430.53	0.47	−0.16	56.0	0.79
3438.23	0.09	0.42	100.0	1.10
3457.56	0.56	−0.53	41.0	0.90
3479.02	0.53	−0.69	25.0	0.65
3479.39	0.71	0.17	55.0	0.69
3499.58	0.41	−0.81	20.0	0.50
3505.67	0.16	−0.36	59.0	0.69
3536.94	0.36	−1.31	11.5	0.64
3573.08	0.32	−1.04	27.0	0.80
3578.23	1.22	−0.61	8.0	0.71
3630.02	0.36	−1.11	22.5	0.79
3714.78	0.53	−0.93	28.0	0.85
3751.60	0.97	0.01	39.0	0.62
3998.97	0.56	−0.67	47.5	0.97
4050.33	0.71	−1.00	16.5	0.76
4090.51	0.76	−1.10	9.0	0.61
4208.99	0.71	−0.46	41.0	0.76
4317.32	0.71	−1.38	10.0	0.86
Nb II, $Z = 41$				
3215.59	0.44	−0.19	Syn	−0.18
Pd I, $Z = 46$				
3242.70	0.81	−0.07	Syn	0.29
3404.58	0.81	0.32	Syn	0.14
3516.94	0.96	−0.24	Syn	0.3:
Ag I, $Z = 47$				
3280.67	0.00	−0.05	Syn	−0.21
3382.90	0.00	−0.38	Syn	−0.36

TABLE 2—*Continued*

λ (Å)	EP (eV)	log *gf*	EW (mÅ)	log ϵ
Ba II, $Z = 56$				
3891.77	2.51	0.28	Syn	0.32
4129.65	2.72	0.56	Syn	0.30
4554.04	0.00	0.17	Syn	0.55
5853.70	0.60	−1.01	Syn	0.40
6141.70	0.60	−0.07	Syn	0.51
6496.90	0.60	−0.38	Syn	0.55
La II, $Z = 57$				
3713.54	0.17	−0.80	9.0	−0.48
3794.77	0.24	0.21	44.0	−0.48
3849.00	0.00	−0.45	28.0	−0.43
3949.10	0.40	0.49	Syn	−0.46
3988.52	0.40	0.21	Syn	−0.46
3995.75	0.17	−0.06	Syn	−0.44
4086.71	0.00	−0.07	Syn	−0.43
4123.22	0.32	0.13	Syn	−0.35
4322.50	0.17	−0.93	10.0	−0.39
4333.75	0.17	−0.06	Syn	−0.49
4429.91	0.23	−0.35	29.5	−0.33
4526.11	0.77	−0.59	3.5	−0.46
4920.96	0.13	−0.58	25.0	−0.37
4921.78	0.24	−0.45	25.5	−0.37
5123.00	0.32	−0.91	Syn	−0.41
Ce II, $Z = 58$				
3539.08	0.32	−0.38	5.5	−0.11
3577.46	0.47	0.21	11.0	−0.21
3940.33	0.32	−0.27	8.0	−0.16
3942.15	0.00	−0.22	16.0	−0.22
3942.74	0.86	0.73	14.5	−0.27
3960.91	0.32	−0.40	6.5	−0.13
3999.24	0.30	0.09	17.0	−0.18
4031.33	0.32	−0.08	11.0	−0.21
4053.50	0.00	−0.71	8.0	−0.10
4073.47	0.48	0.23	14.5	−0.21
4083.22	0.70	0.27	12.5	−0.08
4115.37	0.92	0.10	4.5	−0.16
4118.14	0.70	0.19	8.0	−0.23
4120.83	0.32	−0.21	7.0	−0.31
4127.36	0.68	0.35	11.5	−0.24
4137.65	0.52	0.44	22.0	−0.16
4145.00	0.70	0.13	7.0	−0.24
4165.60	0.91	0.53	13.5	−0.08
4539.74	0.33	−0.02	12.5	−0.26
4562.36	0.48	0.23	19.0	−0.13
4628.16	0.52	0.20	17.0	−0.13
5274.23	1.04	0.15	4.5	−0.20
Pr II, $Z = 59$				
3964.82	0.06	0.12	Syn	−0.65
3965.26	0.20	0.14	Syn	−0.7:
4143.12	0.37	0.61	Syn	−0.69
4179.40	0.20	0.48	Syn	−0.77
4222.95	0.06	0.27	Syn	−0.72
4408.81	0.00	0.18	Syn	−0.73
4510.15	0.42	0.02	5.0	−0.70
5135.14	0.96	0.01	1.5	−0.76
5220.11	0.80	0.30	5.5	−0.71
Nd II, $Z = 60$				
3780.40	0.47	−0.26	10.0	−0.08
3784.25	0.38	0.23	23.5	−0.22

TABLE 2—*Continued*

λ (Å)	EP (eV)	log *gf*	EW (mÅ)	log ϵ
3826.42	0.06	−0.26	13.5	−0.39
3838.98	0.00	−0.18	25.0	−0.20
3865.98	0.06	−0.80	7.5	−0.15
3900.23	0.47	0.20	21.0	−0.17
3973.30	0.63	0.25	17.5	−0.15
4004.01	0.06	−0.59	12.0	−0.15
4013.22	0.18	−1.03	4.0	−0.10
4018.81	0.06	−0.81	8.0	−0.13
4021.34	0.32	0.02	20.5	−0.19
4023.00	0.20	−0.19	17.0	−0.22
4041.06	0.47	−0.70	5.5	0.04
4043.59	0.32	−0.53	8.0	−0.13
4051.15	0.38	−0.21	16.5	−0.02
4059.96	0.20	−0.33	11.0	−0.31
4061.09	0.47	0.40	43.0	0.08
4069.28	0.06	−0.33	15.0	−0.31
4109.45	0.32	0.17	49.5	0.27
4133.36	0.32	−0.45	10.5	−0.09
4446.39	0.20	−0.55	18.5	0.13
4462.99	0.56	−0.06	20.0	0.08
4567.61	0.20	−1.25	3.0	−0.06
4579.32	0.74	−0.55	4.5	0.03
4597.02	0.20	−0.92	5.5	−0.12
4645.77	0.56	−0.59	4.0	−0.19
4859.02	0.32	−0.72	12.0	0.16
5092.79	0.38	−0.59	11.5	0.05
5130.59	1.30	0.20	7.5	0.08
5165.14	0.68	−0.67	8.5	0.32
5200.12	0.56	−0.50	14.0	0.25
5212.35	0.20	−0.76	7.0	−0.23
5234.21	0.55	−0.36	7.5	−0.21
5249.60	0.98	0.12	11.0	−0.02
5255.51	0.20	−0.71	12.0	−0.03
5276.88	0.86	−0.44	3.0	−0.20
5293.17	0.82	−0.08	14.0	0.11
5311.48	0.99	−0.34	2.0	−0.34
5319.82	0.55	−0.24	14.5	−0.01
5361.51	0.68	−0.46	7.0	0.00
Sm II, $Z = 62$				
3896.97	0.04	−0.58	8.5	−0.62
4035.10	0.33	−0.44	6.0	−0.62
4068.32	0.43	−0.71	3.5	−0.49
4206.12	0.38	−1.10	2.5	−0.32
4244.70	0.28	−0.73	4.5	−0.55
4318.94	0.28	−0.27	18.0	−0.34
4329.01	0.18	−0.30	14.0	−0.56
4499.48	0.25	−1.01	4.5	−0.33
4519.63	0.54	−0.43	9.0	−0.27
4523.91	0.43	−0.58	9.5	−0.21
4537.95	0.48	−0.23	8.0	−0.59
4577.69	0.25	−0.77	8.0	−0.31
4642.23	0.38	−0.52	10.5	−0.29
4777.69	0.04	−1.28	4.5	−0.33
4791.60	0.10	−1.23	3.0	−0.50
4815.82	0.18	−0.77	6.5	−0.51
4854.37	0.38	−1.21	2.5	−0.29
Eu II, $Z = 63$				
3724.90	0.00	−0.09	Syn	−0.73
3819.67	0.00	0.51	Syn	−0.69
3907.11	0.21	0.17	Syn	−0.70
3930.50	0.21	0.27	Syn	−0.66
3971.97	0.21	0.27	Syn	−0.72

TABLE 2—*Continued*

λ (Å)	EP (eV)	log *gf*	EW (mÅ)	log ϵ
4129.72	0.00	0.22	Syn	−0.68
4205.05	0.00	0.21	Syn	−0.66
4435.60	0.21	−0.10	Syn	−0.59
6645.13	1.38	0.20	9.0	−0.59
Gd II, $Z = 64$				
3331.40	0.00	−0.14	22.5	−0.27
3439.23	0.38	0.15	18.0	−0.29
3451.23	0.38	−0.05	10.5	−0.38
3481.80	0.49	0.23	18.0	−0.26
3549.37	0.24	0.26	29.0	−0.28
3557.05	0.60	0.21	13.5	−0.28
3697.75	0.03	−0.28	19.5	−0.31
3712.72	0.38	0.15	25.0	−0.21
3768.40	0.08	0.36	46.0	−0.31
3844.58	0.14	−0.40	18.0	−0.14
4037.33	0.66	−0.02	13.5	−0.13
4037.91	0.56	−0.23	7.5	−0.33
4085.57	0.73	0.07	8.0	−0.40
4098.90	0.60	−0.45	6.8	−0.10
4191.08	0.43	−0.57	7.0	−0.17
Tb II, $Z = 65$				
3600.41	0.64	0.61	Syn	−0.92
3658.89	0.13	−0.01	Syn	−0.89
3702.85	0.13	0.44	Syn	−0.89
3848.73	0.00	0.28	Syn	−0.91
3874.17	0.00	0.27	Syn	−0.92
Dy II, $Z = 66$				
3407.80	0.00	0.18	53.5	−0.09
3434.37	0.00	−0.45	25.0	−0.16
3445.57	0.00	−0.15	44.5	−0.01
3454.32	0.00	−0.14	36.0	−0.22
3460.97	0.00	−0.07	37.5	−0.25
3536.02	0.54	0.53	43.0	−0.14
3538.52	0.00	−0.02	50.0	−0.03
3546.83	0.10	−0.55	20.5	−0.10
3550.22	0.59	0.27	30.5	−0.12
3559.30	1.22	−0.28	3.5	−0.01
3563.15	0.10	−0.36	26.5	−0.13
3694.81	0.10	−0.11	45.0	−0.07
3747.82	0.10	−0.81	18.5	0.01
3788.44	0.10	−0.57	25.0	−0.06
3983.65	0.54	−0.31	17.0	−0.09
3996.69	0.59	−0.26	16.0	−0.12
4073.12	0.54	−0.32	19.5	−0.02
4077.96	0.10	−0.04	53.5	−0.05
4449.70	0.00	−1.03	18.0	0.00
Ho II, $Z = 67$				
3810.72	0.00	0.14	Syn	−0.8:
3891.72	0.08	0.45	Syn	−0.8:
4045.44	0.08	−0.18	Syn	−0.5:
Er II, $Z = 68$				
3499.10	0.05	0.14	50.0	−0.18
3559.90	0.00	−0.74	14.5	−0.23
3692.65	0.05	0.14	56.0	−0.18
3786.84	0.00	−0.64	Syn	−0.10
3830.48	0.00	−0.36	36.0	−0.20
3896.23	0.05	−0.24	Syn	−0.18
3938.63	0.00	−0.52	Syn	−0.30

TABLE 2—*Continued*

λ (Å)	EP (eV)	log *gf*	EW (mÅ)	log ϵ
Tm II, $Z = 69$				
3700.26	0.03	−0.29	Syn	−1.0:
3848.01	0.00	−0.13	Syn	−1.10
Os I, $Z = 76$				
2838.63	0.00	0.11	Syn	0.5:
3018.04	0.00	−0.72	Syn	0.45
3058.66	0.00	−0.43	Syn	0.45
3267.95	0.00	−1.08	Syn	0.5:
3301.57	0.00	−0.75	Syn	0.4:
Ir I, $Z = 77$				
3220.76	0.35	−0.51	Syn	0.45
3513.65	0.00	−1.26	Syn	0.25
3800.12	0.00	−1.45	Syn	0.20
Pt I, $Z = 78$				
2646.88	0.00	−0.73	Syn	0.70
2650.85	0.10	−0.95	Syn	0.70
2659.45	0.00	−0.07	Syn	0.67
2929.79	0.00	−0.80	Syn	0.55
3064.71	0.00	−0.34	Syn	0.7:
Au I, $Z = 79$				
2675.94	0.00	−0.46	Syn	−0.3:
Pb I, $Z = 82$				
2833.05	0.00	−0.68	Syn	0.4:
3639.81	0.97	−0.72	Syn	<0.8
3683.46	0.97	−0.60	Syn	<0.6
4057.81	1.32	−0.17	Syn	<0.4
Th II, $Z = 90$				
4019.12	0.00	−0.27	Syn	−1.18
4086.52	0.00	−0.89	Syn	−1.1:
U II, $Z = 92$				
3859.57	0.04	−0.17	Syn	≤−1.7

NOTE.—Table 2 is also available in machine-readable form in the electronic edition of the *Astrophysical Journal*.

sidering that much of the improved atomic transition data had not been published at the time of the analysis of Johnson & Bolte (2001) and that their results were based on far fewer lines per element than we have used. The comparison with Burris et al. (2000) for eight *n*-capture elements seems at first glance to be much worse: $\langle\Delta[n\text{-capture/Fe}]\rangle = 0.25 \pm 0.06$ ($\sigma = 0.18$). However, the spectroscopic resolution for that study ($R \simeq 30,000$) was much less than the resolutions of our Keck and McDonald data, making fewer transitions available for analysis. Burris et al. (2000) determined abundances from only one to two lines per element and assumed a larger microturbulent velocity ($v_t = 2.3$ km s^{-1}) than we recommend ($v_t = 1.9$ km s^{-1}). The v_t choice strongly affects the abundances derived from Sr II and Ba II lines. If we neglect those two elements and also Nd, whose abundance is subject to large uncertainties from its atomic transition data, then the comparison is much better for the

TABLE 3
NEUTRON CAPTURE ELEMENT ABUNDANCES FOR BD +17°3248

			McDONALD, KECK				*HST*/STIS			
SPECIES	Z	$\log \epsilon_\odot$[a]	$\log \epsilon$	σ[b]	Number	[M/Fe]	$\log \epsilon$	σ[b]	Number	[M/Fe]
Ge I	32	3.41	...	...	...	...	0.60	(0.15)	1	−0.72
Sr I	38	2.90	0.90	(0.15)	1	0.09	...	...	...	...
Sr II	38	2.90	1.10	(0.10)	2	0.29	...	...	...	...
Y II	39	2.24	0.04	0.05	11	−0.11	...	...	...	...
Zr II	40	2.60	0.76	0.14	19	0.25	0.65	0.13	5	0.14
Nb II	41	1.42	−0.18	(0.15)	1	0.49	...	...	...	...
Pd I	46	1.69	0.24	0.09	3	0.64	...	...	...	...
Ag I	47	1.24	−0.28	0.11	2	0.57	...	...	...	...
Ba II	56	2.13	0.44	0.11	6	0.40	...	...	...	...
La II	57	1.22	−0.42	0.05	15	0.45	...	...	...	...
Ce II	58	1.55	−0.18	0.06	22	0.36	...	...	...	...
Pr II	59	0.71	−0.71	(0.05)	9	0.67	...	...	...	...
Nd II	60	1.50	−0.07	0.17	40	0.52	...	...	...	...
Sm II	62	1.00	−0.42	0.14	17	0.67	...	...	...	...
Eu II	63	0.51	−0.67	0.05	9	0.91	...	...	...	...
Gd II	64	1.12	−0.26	0.09	15	0.71	...	...	...	...
Tb II	65	0.33	−0.91	(0.05)	5	0.85	...	...	...	...
Dy II	66	1.10	−0.03	0.07	19	0.96	...	...	...	...
Ho II	67	0.50	−0.70	0.17	3	0.89	...	...	...	...
Er II	68	0.93	−0.20	0.06	7	0.96	...	...	...	...
Tm II	69	0.13	−1.07	(0.10)	2	0.89	...	...	...	...
Os I	76	1.45	0.45	(0.10)	2	1.1:	0.47	(0.05)	3	1.11
Ir I	77	1.30	0.30	0.13	3	1.09	...	...	...	...
Pt I	78	1.80	...	...	...	...	0.67	0.07	5	0.96
Au I	79	0.83	...	...	...	...	−0.3:	(0.30)	1	0.8:
Pb I	82	1.85	...	...	...	...	<0.3	0.25	2	<0.5
Th II	90	0.12	−1.18	(0.10)	2	0.79	...	...	...	...
U II	92	−0.07	−2.0:	(0.30)	1	0.0:	...	...	...	...

[a] Taken from Grevesse & Sauval 1998.

[b] For a species with three or more lines, the σ entry is the maximum of the measured sample standard deviations or 0.05. If there are two lines, the entry is the greater of the true σ or 0.10, and if only one line has been used, the entry is the greater of the true σ or 0.15. For any of these cases, if an arbitrary minimum value of 0.05, 0.10, or 0.15 is entered, then it is enclosed in parentheses.

other remaining five elements in common: $\langle \Delta[n\text{-capture/Fe}] \rangle = 0.14 \pm 0.04$ ($\sigma = 0.09$).

In Figures 3–8 we present a series of small spectral regions surrounding some key *n*-capture transitions. The top panels of each of these figures compare the observed spectra of BD +17°3248 to that of HD 122563, and the bottom panels match synthetic and observed spectra just of BD +17°3248. Inspection of these figures reveals that the line strengths of the two stars generally are comparable, as the ~700 K cooler $T_{\rm eff}$ of HD 122563 strengthens its absorption spectrum enough to roughly compensate for its ~0.6 dex lower metallicity. In a few instances an atomic or molecular line is stronger in the HD 122563 spectrum than it is in BD +17°3248, as a result of a particular combination of excitation/ionization conditions of the transition. However, far more often some lines are much stronger in the BD +17°3248 spectrum; these are the signs of very large abundances of most *n*-capture elements in this star.

Some comments should be given here on general *n*-capture abundance results. Consider first "rare earth" elements, defined as those of the lanthanide group (La → Lu, $57 \leq Z \leq 71$) plus Ba ($Z = 56$). They are linked not only by consecutive atomic numbers in the periodic table but also by spectroscopic species availability. Rare earth elements have low first ionization potentials (IP ≤ 6.2 eV), so these elements exist almost entirely as singly ionized species in cool metal-poor giants: $N_{\rm Xtot} \simeq N_{\rm XII}$. Thus, the "Saha corrections" for other ionization stages are negligible. Additionally, the detectable transitions arise predominantly from low-lying excitation states (usually EP < 1.0 eV) of these ions. Therefore, the Boltzmann exponential factors essentially cancel out for abundance ratios among the rare earth elements. Derived ratios such as, e.g., $\log \epsilon$(La/Dy), are nearly independent of $T_{\rm eff}$ and $\log g$ uncertainties in BD +17°3248.

The mean of the measured line-to-line scatters σ of the rare earth elements given in Table 3 (ignoring the σ values arbitrarily defined for Pr, Tb, and Tm) is not large: $\langle \sigma \rangle = 0.10$. It would reduce to 0.08 if we neglect the values for Nd (see the discussion in the Appendix) and Ho (whose abundance is based on three lines, two of which are badly blended). Undoubtedly the mean σ would shrink further with careful reexamination of some obvious outlying abundance points for a few elements. The insensitivity of rare earth element abundance ratios and the availability of excellent atomic data for these elements combine to yield a very accurate "complete" abundance distribution of rare earth elements in BD +17°3248. The entire set of these elements is greatly enhanced, reaching a maximum of [*n*-capture/Fe] ≃ 0.9 for atomic numbers $Z > 60$.

The abundances of lighter *n*-capture elements (Ge → Ag, $32 \leq Z \leq 71$) are less overabundant, and the abundance

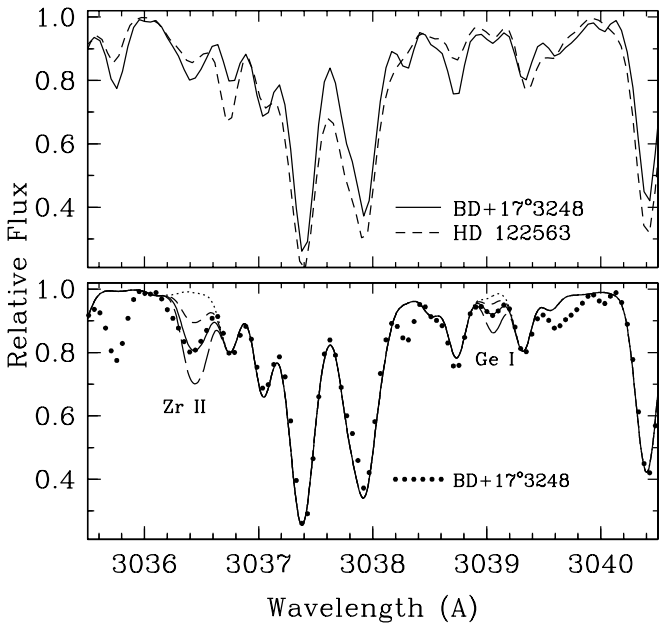

FIG. 3.—Observed *HST*/STIS and synthetic spectra in region surrounding the Zr II λ3036.39, Zr II λ3036.52, and Ge I λ3039.07 lines. In the top panel, the observed BD +17°3248 spectrum is compared to that of HD 122563. In the bottom panel, the observed BD +17°3248 spectrum is compared to four synthetic spectra, shown in order of increasing abundance of Zr and Ge by dotted, short-dashed, solid, and long-dashed lines computed for these abundances: $\log \epsilon(\mathrm{Zr}) = -\infty$, 0.30, 0.70, and 1.10 and $\log \epsilon(\mathrm{Ge}) = -\infty$, 0.20, 0.60, and 1.00.

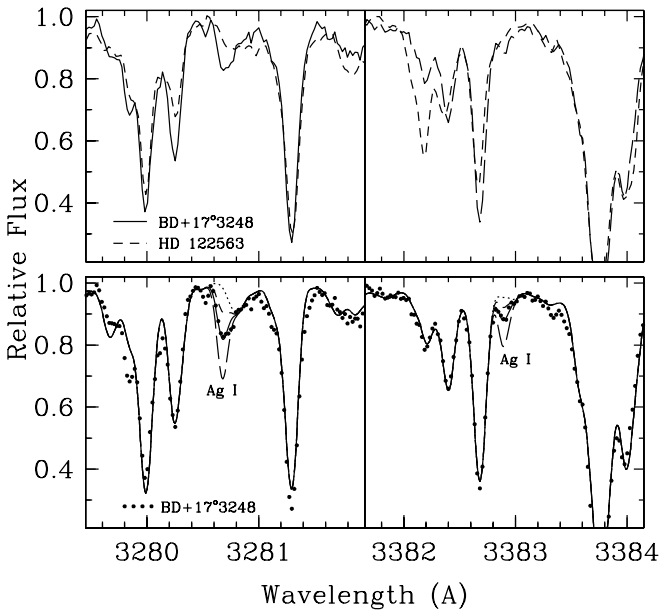

FIG. 4.—Observed Keck/HIRES and synthetic spectra in region surrounding the Ag I λλ3280.67 and 3382.90 lines, in the manner of Fig. 3. In the bottom panel, the synthetic spectra were computed for abundances $\log \epsilon(\mathrm{Ag}) = -\infty$, −0.68, −0.28, and 0.12.

enhancements apparently vary directly with atomic number. The lightest of these elements, Ge, is in fact very *underabundant* in BD +17°3248: [Ge/Fe] ∼ −0.7. This effect can be seen in Figure 3, which in the top panel overlays the observed spectra of BD +17°3248 and HD 122563 surrounding the Ge I λ3039.07 line and in the bottom panel shows a comparison between synthetic and observed spectra of that wavelength region in BD +17°3248. If [Ge/Fe] were actually ∼0, then the Ge I line would be stronger, not weaker, than the two lines bracketing it 0.3 Å to the blue and to the red.

The abundances of the Sr → Zr group ($38 \leq Z \leq 40$) are at best weakly overabundant with respect to Fe (this is similar to some other *r*-process–rich stars, such as HD 115444; see, e.g., Figs. 4 and 5 of Westin et al. 2000). Both Sr I and Sr II lines have been analyzed, and neither species indicates an anomalously large abundance.[15] Additionally, the very modest positive [Zr/Fe] ratio derived from 19 Zr II transitions appearing on our ground-based spectra is confirmed by five lines of this species appearing on our *HST*/STIS spectrum; see some of the UV Zr II lines in Figures 3 and 6.

Elements in the $Z = 41$–47 range are more overabundant with respect to Fe. Synthetic and observed spectra of the two Ag I resonance lines are presented in Figure 4, revealing cleanly detected features that are relatively easy to analyze. The Ag I lines are the resonance transitions, which have well-known *gf*-values and hyperfine/isotopic structure information. The major surrounding contaminant atomic and NH molecular features can be modeled to good approximation. Therefore, the derived Ag abundance should be reliable.

Detected transitions of third *n*-capture peak elements (Os → Pb, $76 \leq Z \leq 82$) have several common properties: they all arise from low-excitation states of the neutral species; they generally occur at very short wavelengths, $\lambda \lesssim 3800$ Å; and they are mostly weak lines that suffer blending from other atomic and molecular (mostly OH and NH) features. Fortunately, transition probabilities for these lines are generally known to good accuracy, and the abundance analysis limitation lies mostly with line detection and modeling of contaminant spectral features. Some of the details involved in line selection for these elements have been discussed by Sneden et al. (1998); the Appendix provides additional information.

The *HST*/STIS spectra of two Pt I lines are displayed in Figure 5, and one of the Os I lines is given in Figure 6. The top panels of these two figures show very clearly the presence of absorption lines of third *n*-capture peak species in BD +17°3248 and their undetectability in HD 122563. The fits of synthetic to the observed spectra of BD +17°3248 displayed in the bottom panels confirm the conclusions of the visual comparison of the two stars.

Abundances of third *n*-capture peak elements Os, Ir, Pt, and Au in BD +17°3248 are very consistent: $[\langle \mathrm{Os, Ir, Pt, Au} \rangle / \mathrm{Fe}] = 0.99 \pm 0.07$ ($\sigma = 0.14$). This mean overabundance is slightly larger than that of the rare earth elements whose solar system abundances are dominated by the *r*-process: $[\langle \mathrm{Eu} \rightarrow \mathrm{Tm} \rangle / \mathrm{Fe}] = 0.88 \pm 0.03$ ($\sigma = 0.07$), but the difference is hardly more than the combined standard deviations. This ∼0.1 dex offset may be a real abundance effect, but it possibly could be simply an uncertainty in our abundance computations. Recall that the third *n*-cap-

[15] The abundance derived from the single detected Sr I line is 0.2 dex smaller than that from the two Sr II lines. However, the ionized lines are the two extremely strong resonance transitions on the flat/damping region of the curve of growth [$\log(\mathrm{EW}/\lambda) \simeq -4.4$], and Sr abundances derived from them are very sensitive to the adopted v_t value. The error bars of Sr abundances derived from neutral and ionized lines overlap.

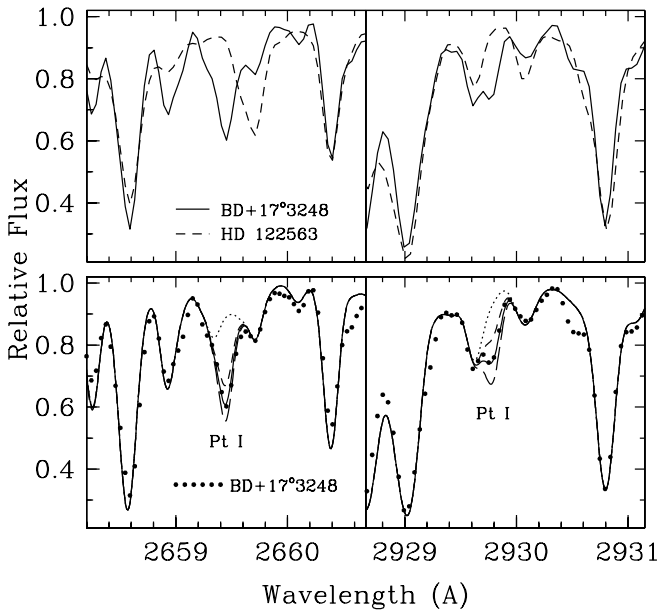

FIG. 5.—Observed *HST*/STIS and synthetic spectra in region surrounding the Pt I $\lambda\lambda$2659.45, 2929.78 lines, in the manner of Fig. 3. In the bottom panel, the synthetic spectra were computed for abundances $\log \epsilon(\mathrm{Pt}) = -\infty$, 0.27, 0.67, and 1.07.

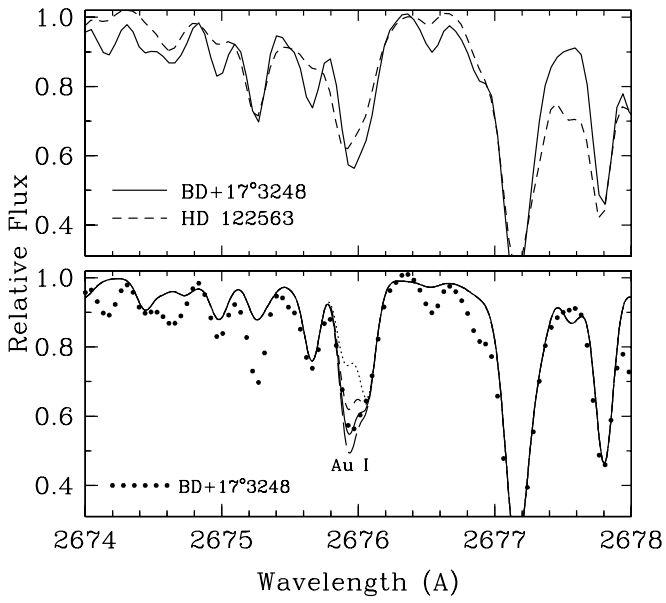

FIG. 7.—Observed *HST*/STIS and synthetic spectra in region surrounding the Au I λ2675.94 line, in the manner of Fig. 3. In the bottom panel, the synthetic spectra were computed for abundances $\log \epsilon(\mathrm{Au}) = -\infty$, −0.82, −0.32, and 0.18.

ture peak abundances have been derived from neutral-species transitions, while those of the rare earth elements have been derived from ionized-species lines. Thus, uncertainties in $T_{\rm eff}$ and $\log g$ enter into ionization equilibrium computations. While the estimated uncertainties of $\pm$150 K in $T_{\rm eff}$ and $\pm$0.3 in $\log g$ produce no changes larger than $\simeq$0.02 in abundance ratios $\log \epsilon$(rare earth/rare earth) or $\log \epsilon$(third peak/third peak), the temperature uncertainty yields an uncertainty of $\mp$0.08 in $\log \epsilon$(third peak/rare earth), and a gravity uncertainty leads to $\pm$0.12 (see also § 3.5 of S96 and § 3.1 of Westin et al. 2000). Therefore, a small increase in $T_{\rm eff}$ or a small decrease in $\log g$ could make the ∼0.1 offset between the abundances of third peak and rare earth elements disappear. Note that the slightly higher abundances of third peak elements with respect to the rare earth elements make it unlikely that departures from LTE in the form of overionization are causing the small offset between the two element groups.[16]

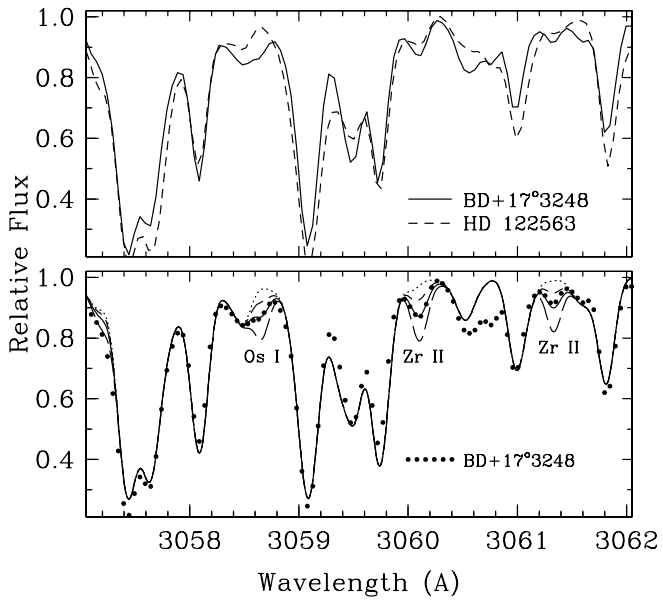

FIG. 6.—Observed *HST*/STIS and synthetic spectra in region surrounding the Zr II λ3060.11, Zr II λ3061.33, and Os I λ3058.66 lines, in the manner of Fig. 3. In the bottom panel, the synthetic spectra were computed for abundances $\log \epsilon(\mathrm{Zr}) = -\infty$, 0.30, 0.70, and 1.10 and $\log \epsilon(\mathrm{Os}) = -\infty$, 0.05, 0.45, and 0.95.

We have detected gold in the STIS spectrum of BD +17°3248. In the top panel of Figure 7 we plot observed spectra of the Au I λ2675.94 resonance line BD +17°3248 and HD 122563, and in the bottom panel of this figure we compare observed and synthetic spectra of BD +17°3248 alone. There is little obvious difference between the spectra of BD +17°3248 and HD 122563 at 2676.0 Å, but we believe that this is due to the complex set of absorption lines that contribute to the total feature at this wavelength. The Au I λ2675.94 line is blended by OH λ2675.89, Ta II λ2675.90, Nb II λ2675.94, Ti I λ2676.07, and Mn I λ2676.09. In particular, OH has strong absorption lines throughout the UV spectrum of HD 122563, leading in this case to a deep λ2676.0 feature. In BD +17°3248 the OH absorption does not disappear, but it is much less prominent. To determine an abundance for Au, we must also deal with the other atomic contaminants. We did not determine an abundance for Ta, but Burris et al. (2000) suggest that the *r*-process fraction of this element in solar system material is 0.60. This roughly equal split between *r*- and *s*-process contributions is similar to those of rare earth elements Ce, Pr, and Nd, and so we estimated for BD +17°3248 that $\log \epsilon$(Ta)

[16] The first ionization potentials of Os, Ir, Pt, and Au are larger than those of most other metals, averaging ∼8.9 eV. Radiative ionization of these species would require very energetic UV photons, which are not in plentiful supply in our program stars.

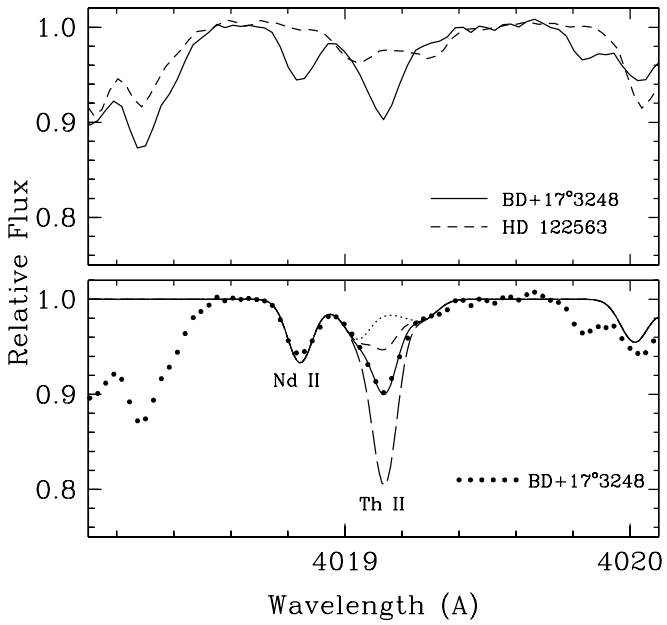

FIG. 8.—Observed Keck/HIRES and synthetic spectra in region surrounding the Th II λ4019.12 line, in the manner of Fig. 3. In the bottom panel, the synthetic spectra were computed for abundances $\log \epsilon(\mathrm{Th}) = -\infty, -1.58, -1.18$, and -0.78.

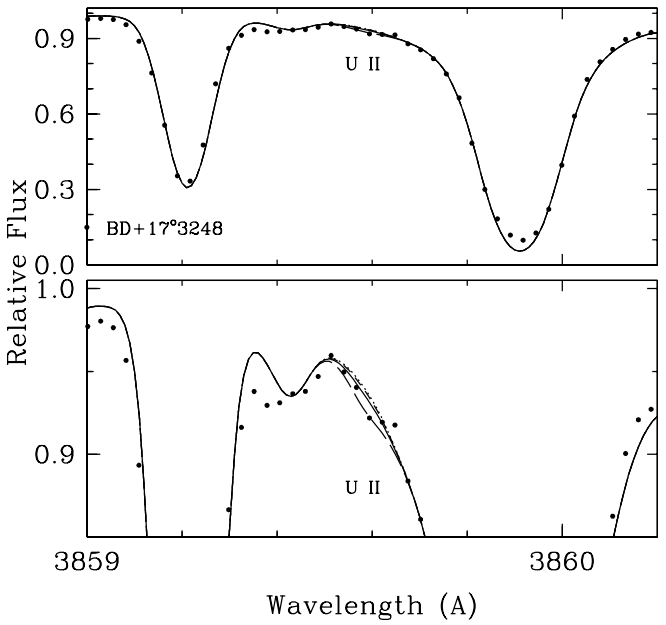

FIG. 9.—Spectra of BD +17°3248 in region surrounding the U II λ3859.57 line. In both panels the observed Keck/HIRES spectrum is compared to four synthetic spectra computed for abundances $\log \epsilon(\mathrm{U}) = -\infty, -2.60, -2.10$, and -1.60. (Note that some of the lines overlap.) The only difference between the two panels is the vertical scale, which is expanded in the bottom panel for easier assessment of the extremely weak U II feature.

$\simeq \log \epsilon(\mathrm{Ta})_{\odot} - [\mathrm{Fe/H}] + [\langle \mathrm{Ce, Pr, Nd} \rangle / \mathrm{Fe}] \simeq 0.13 - 2.09 + 0.6 \simeq -1.4$. The resulting Ta and Nb absorptions account for about half of the total feature strength at 2675.9 Å. The derived Au abundance is thus vulnerable to abundance or transition probability uncertainties in Ta and Nb. Comments on the other Au I resonance line at 2427.94 Å appear in the Appendix.

The third *n*-capture peak element Pb merits an additional comment. We are unable to detect the Pb I lines at 3683.46 and 4057.81 Å in our ground-based spectra of BD +17°3248. The λ2833.05 line should be much stronger, and indeed there is detectable absorption near this wavelength in the *HST*/STIS spectrum. Frustratingly, the observed line centroid lies about 0.03 Å redward of the predicted Pb I line, and there is an Fe II line with a known laboratory *gf* that appears to account for the majority of the strength of the combined feature. We have listed a rough estimate of the Pb abundance from this line in Table 2, but the upper limits derived from the longer wavelength lines provide just as reliable a Pb abundance; hence, we suggest in Table 3 that $\log \epsilon(\mathrm{Pb}) \lesssim 0.3$.

The well-studied Th II λ4019.12 line is easily detected in BD +17°3248, while in HD 122563 the Th II line is lost amid other absorbers at this wavelength (see the top panel of Fig. 8). Details of the analysis of this line have been discussed in several studies (Morell, Källander, & Butcher 1992; François, Spite, & Spite 1993; S96; Norris, Ryan, & Beers 1997; Westin et al. 2000; Johnson & Bolte 2001). We can add little to the discussion in those papers, but we emphasize from inspection of the synthetic spectra given in the bottom panel of Figure 8 that BD +17°3248 has a fairly clean Th II feature and the derived Th abundance is not very sensitive to the modeling of the contaminants. The ratio of Th to the rare earth elements is determined to high accuracy.

We also suggest from syntheses of the U II λ3859.60 line (Fig. 9) that it is possibly detected in BD +17°3248. The line is of course extremely weak, and to maximize its visibility we have experimented with spectral deconvolution of the Keck/HIRES spectrum in this wavelength region. The deconvolution was done according to the algorithm of Gilliland et al. (1992), with the purpose of restoring the true spectral resolution limit of the data. Such an operation of course decreases the S/N per pixel as it increases the resolution. The observed spectrum in Figure 9 is the result of the deconvolution process, but the very weak U II line appears to be present in both the original and deconvolved spectrum of BD +17°3248. Naturally, the derived U abundance has an associated error estimate that is much larger than that of most other *n*-capture elements.

4. DISCUSSION

4.1. *Neutron Capture Element Abundances*

Our Keck and *HST* observations have provided abundance determinations for a wide range in proton number, from Ge to U. This is currently the largest range of *n*-capture elements detected in any metal-poor halo stars.

4.1.1. *Heavier Elements* ($Z \geq 56$)

Abundance determinations in a number of Galactic halo and globular cluster stars have shown that the rare earth elements, roughly from barium to hafnium, are consistent with a scaled (i.e., adjusted for metallicity) solar system *r*-process distribution (see, e.g., S96; Cowan et al. 1999; B00; Sneden et al. 2000a, 2000b; Johnson & Bolte 2001). Isotopic abundances for europium in metal-poor halo stars also indicate a solar system pattern, as shown in Sneden, Lawler, & Cowan (2001b) and Sneden et al. (2002). Examination of Figure 10,

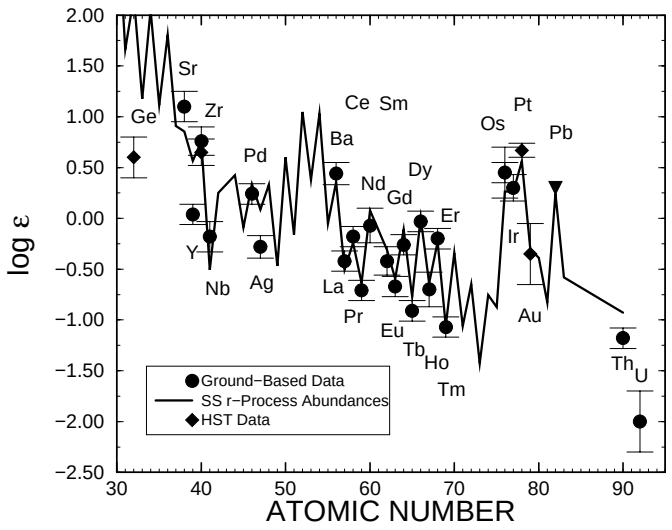

FIG. 10.—Neutron capture element abundances in BD +17°3248, obtained by ground-based and *HST* observations, compared to a scaled solar system *r*-process abundance curve. The upper limit on the lead abundance is denoted by an inverted triangle. Note also the thorium and uranium detections. [*See the electronic edition of the Journal for a color version of this figure*.]

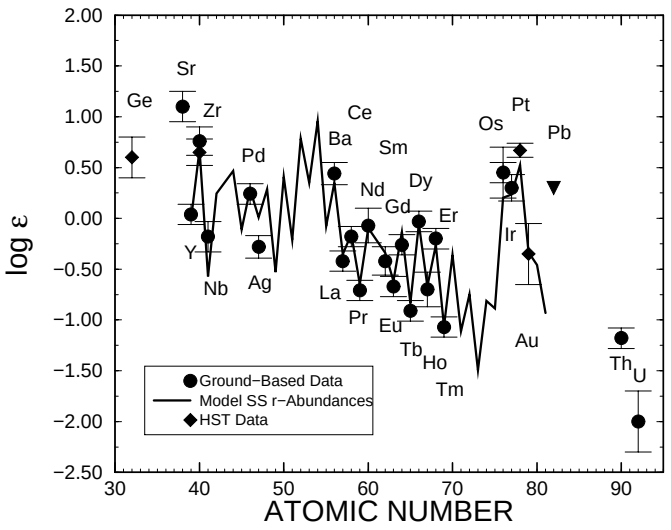

FIG. 11.—Same as Fig. 10, except the scaled solar system *r*-process curve is based on the stellar *s*-process model of Arlandini et al. (1999). [*See the electronic edition of the Journal for a color version of this figure*.]

where the solid line denotes the solar system *r*-process–only elemental abundances, again shows that same pattern. What is different about this star, however, is that the *HST* observations demonstrate that the third *r*-process peak elemental abundances (now including gold and the upper limit on lead) appear to follow the rare earth pattern and fall on the same matching abundance distribution. There is some indication, however, that a few of the elements, for example, Os, in the third *r*-process peak may be slightly higher (on the order of 0.1 dex, which is the typical elemental abundance uncertainty) than the matching solar system *r*-process curve. As noted earlier in § 3.3, this small offset may be a real effect or may result from uncertainties in our abundance computations—the difference between abundances of neutral and ionized species. We note further that while Os appears somewhat high, Ir and Au fall precisely on the curve, and that seems to point to an overall agreement with the rare earth region. There have been suggestions of this agreement before in the observations of HD 115444 (Westin et al. 2000) and CS 22892-052 (Sneden et al. 2000a), but these new combined (ground- and space-based) observations of BD +17°3248 have provided greater access to the heaviest stable *n*-capture elements than previously possible, with presumably more reliable abundance determinations.

The solid line illustrated in Figure 10 was derived by summing the individual isotopic contributions from the *s*- and the *r*-process in solar system material, as determined by Käppeler, Beer, & Wisshak (1989) and Wisshak, Voss, & Käppeler (1996) from *n*-capture cross section measurements. This solar *r*-process, and corresponding *s*-process, elemental distribution was first published in S96 and later updated in B00. The deconvolution of the solar system material into the *s*-process and *r*-process relied on reproducing the "σN" curve (i.e., the product of the *n*-capture cross section and *s*-process abundance). This "classical approach" to the *s*-process is empirical and by definition model independent. More sophisticated models, based on *s*-process nucleosynthesis in low-mass AGB stars, have been developed recently. In Figure 11 we again compare the abundances of elements in BD +17°3248 with a solar *r*-process curve. However, in this case the curve has been obtained by summing the solar *r*-process isotopic residuals from the stellar *s*-process model of Arlandini et al. (1999). (Note that Sr and Pb are not included in this distribution.) As is seen in this figure, the agreement between this "model" solar system *r*-process curve and the rare earth abundances in BD +17°3248 is slightly better than the fit of stellar abundances to the standard *r*-process curve shown in Figure 10. For the 13 elements with $56 \leq Z \leq 69$, the mean abundance comparison with the Arlandini et al. (1999) *r*-process solar distribution is $\langle \Delta(\log \epsilon) \rangle \equiv \langle \log \epsilon_{\rm BD\ +17^\circ 3248} - \log \epsilon_{\rm solar} \rangle = 0.395 \pm 0.017$ ($\sigma = 0.062$). In the comparison of BD +17°3248 abundances with the standard solar *r*-process curve the mean difference is nearly the same but the scatter of individual points is somewhat larger: $\langle \Delta(\log \epsilon) \rangle = 0.408 \pm 0.024$ ($\sigma = 0.082$).

The agreement between the heavier *n*-capture elements and the scaled solar system *r*-process curve in this star, as well as in several other stars, suggests that the *r*-process is robust for the upper end. This in turn puts constraints on possible sites for the *r*-process—something that is not known with certainty—and on the conditions under which it operates. This robustness, for example, might suggest a narrow range of supernova masses (e.g., Mathews, Bazan, & Cowan 1992; Wheeler, Cowan, & Hillebrandt 1998) or perhaps well-confined conditions for *r*-process nucleosynthesis in a supernova environment (e.g., Cameron 2001).

In Figures 10 and 11 it can be seen that Ba (an element that is usually thought of as an *s*-process element and is predominantly produced by that process in solar system material) was, instead, synthesized by the *r*-process in BD +17°3248. These results support earlier suggestions (Truran 1981) and the results of larger surveys (McWilliam et al. 1995a, 1995b; McWilliam 1998; B00) of an *r*-process origin for this element early in the history of the Galaxy. It is also evident for BD +17°3248 that not only Ba but all the other so-called *s*-process elements appear to have been synthe-

sized early in the history of the Galaxy by the *r*-process, a result similar to that found for the individual UMP stars CS 22892-052 and HD 115444. The presence of this *r*-process material in metal-poor stars such as BD +17°3248 and old halo stars, including the heaviest *r*-process elements, also places constraints on the earliest stellar generations, in particular, suggesting rapidly evolving progenitors of the halo stars. This follows since the early Galaxy appears to be chemically inhomogeneous in *n*-capture elements (B00; Sneden, Cowan, & Truran 2001a; Cowan, Sneden, & Truran 2001), implying a relatively short (with respect to stellar evolutionary) timescale between the death of the progenitors and the formation of the halo stars. As an example of the scatter seen in the early Galaxy at low metallicity, BD +17°3248 with $[Fe/H] = -2.0$ has a value of $[Eu/Fe] = 0.85$, significantly above the solar value.

4.1.2. *Lighter Elements* ($30 < Z < 55$)

Our new observations of BD +17°3248 have demonstrated the presence of Nb, Pd, and Ag. This is the second metal-poor halo star, after CS 22892-052, with derived abundances for several elements in the domain $40 < Z < 56$, along with abundances of nearly all rare earth elements. Examination of Figure 10 indicates that the abundances of these three lighter *n*-capture elements are not consistent with the same solar *r*-process curve that matches the heavier *n*-capture elements, i.e., $Z \geq 56$. These observations of BD +17°3248, along with those in CS 22892-052, are consistent with earlier suggestions—based on analyses of solar system meteoritic material—that there may be two sites for the *r*-process with the heavier elements (Ba and above) produced in more rapidly occurring events and the lighter elements in less commonly occurring syntheses (Wasserburg, Busso, & Gallino 1996; Wasserburg & Qian 2000). Alternatively, a combination of *r*-process nucleosynthesis in supernovae and in neutron star binaries (Rosswog et al. 1999), with different sites responsible for different ends of the abundance distribution, is also possible. Sneden et al. (2000a) suggested that the total *n*-capture abundance pattern in CS 22892-052, similar to what we now find in BD +17°3248, could also be consistent with a neutrino-heated supernova ejecta *r*-process in a single supernova event, with two different epochs in the explosion/ejection process. Some studies (see, e.g., Pfeiffer et al. 2001a; Pfeiffer, Ott, & Kratz 2001b) were able to reproduce the total abundance pattern found in CS 22892-052 in the context of a single site. We emphasize that the heavier *n*-capture elements, which follow the scaled solar system *r*-process curve, all seem to be produced in one site, or at least under similar conditions, making this a robust process. Thus, for those elements a second *r*-process site (such as merging neutron star binaries) is not required. Further, the necessity of such a site, even for the lighter *n*-capture elements below barium, has also been called into question. It has been proposed that both ends of the abundance distribution could be synthesized in different regions of the same neutron-rich jet of a core collapse supernova (Cameron 2001). Clearly, additional stellar observational data for elements below barium will be important in helping to resolve this question.

As seen in Figure 10, the abundances of the elements Sr, Y, and Zr in BD +17°3248 also do not follow the solar *r*-process curve that matches the heavier *n*-capture elements. This is not surprising, as detailed abundance studies of several other stars, e.g., CS 22892-052 (Sneden et al. 2000a), HD 115444 (Westin et al. 2000), and HD 122563 (Sneden et al. 1998), have all shown this disparity. The production of the elements Sr, Y, and Zr, however, may be complicated since they could be produced not only in the *r*-process but in the weak *s*-process occurring in massive stars (Raiteri et al. 1993). Thus, some combination of those processes could be responsible for the abundance pattern we observe in BD +17°3248. Figure 11, though, suggests that more sophisticated *s*-process models, such as those of Arlandini et al. (1999), might be more successful in explaining the abundances, so far, of Y and Zr in stars such as BD +17°3248.

We note, finally, that the Ge abundance falls well below the solar curve. This element has been seen previously in only three other metal-poor halo stars, and in all cases the Ge abundance exhibited the same behavior (Sneden et al. 1998). Interestingly, in those other cases the Ge abundance seems to scale, at least weakly, with the iron abundance. Thus, the Ge abundance in both HD 115444 and HD 122563, stars with $[Fe/H] \simeq -3$, was the same. HD 126238, with a factor of about 20 higher in metallicity, has a Ge abundance about a factor of 16 higher than in the first two stars. The Ge abundance for BD +17°3248, with $[Fe/H] = -2$, is consistent with that pattern, falling between those of HD 115444 and HD 122563 and the more metal-rich HD 126238. The scaling is not exact, however. We are currently examining this possible weak metallicity dependence, as well as possible nucleosynthetic explanations for this behavior (J. W. Truran et al. 2002, in preparation).

4.2. *Radioactive Age Determinations*

Our new observations indicate the presence of thorium in BD +17°3248. This adds to the growing list of such Th detections in metal-poor and UMP stars (e.g., S96; Sneden et al. 2000a; Westin et al. 2000; Johnson & Bolte 2001; Cayrel et al. 2001). These detections, therefore, allow for chronometric stellar age estimates, typically by comparing the observed stellar abundance ratio Th/Eu with predictions of the initial (zero-decay) value of Th/Eu at the time of the formation of these elements. (Eu is employed since it is also a predominantly *r*-process element and has spectral features that are easily observed in most metal-poor stars.)

The very recent, and first, detection of uranium in the UMP star CS 31082-001 ($[Fe/H] = -2.9$) by Cayrel et al. (2001) offers promise for these stellar age detections with the addition of a second chronometer. The spectrum of BD +17°3248 indicates the presence of uranium, albeit weakly (see Fig. 9), marking this as the second metal-poor halo star in which U has been detected. Such detections may, however, turn out to be uncommon as previous observations have failed to detect U in such stars as CS 22892-052 and HD 115444 (see also Burles et al. 2001 for further discussion).

Cayrel et al. (2001; see also Toenjes et al. 2001) employed the abundances of U and Th, in combination with each other and with some other stable elements, to find an average chronometric age of 12.5 ± 3 Gyr for CS 31082-001. To make these age calculations, they relied mostly on the predicted initial (zero-decay) values listed in Cowan et al. (1999), based on the extended Thomas-Fermi model with quenched shell effects far from stability, i.e., ETFSI-Q (see Pfeiffer et al. 1997 for discussion). Predictions for initial

TABLE 4
CHRONOMETRIC AGE ESTIMATES FOR BD +17°3248

Chronometer Pair	Predicted	Observed	Age (Gyr)	Solar[a]	Lower Limit (Gyr)
Th/Eu	0.507	0.309	10.0	0.4615	8.2
Th/Ir	0.0909	0.03113	21.7	0.0646	14.8
Th/Pt	0.0234	0.0141	10.3	0.0323	16.8
Th/U	1.805	7.413	≥13.4	2.32	11.0
U/Ir	0.05036	0.0045	≥15.5	0.0369	13.5
U/Pt	0.013	0.0019	≥12.4	0.01846	14.6

[a] From Burris et al. 2001.

abundance ratios of Th/Eu, or Th to other stable elements, have been necessary since the nuclei involved in the *r*-process are far from stability, and nuclear data have not in general been available. That situation has been slowly changing, however, with more nuclear data leading to increasingly more reliable prescriptions for very neutron-rich nuclei (see Pfeiffer et al. 2001a; Burles et al. 2001).

We have employed the Th/U abundance ratio, similarly to Cayrel et al. (2001), to make age calculations for BD +17°3248. The uranium detection in BD +17°3248, however, is quite weak and has a relatively large error bar. One possible interpretation of our data is that we are, in fact, only measuring the upper limit on that abundance, an alternative we consider below. As in other previous studies, we have also included chronometric age estimates for BD +17°3248 based on the Th/Eu ratio. In addition, our *HST* observations have provided the abundances of the important third *r*-process peak elements, particularly Pt. These (heaviest stable) elements are closer in nuclear mass number to Th and U than Eu, for example, and thus offer a direct comparison with ratios of Th or U to less massive *n*-capture elements. Similarly to Cayrel et al. (2001), we have made use of the predicted initial (zero-decay) abundance ratios from Cowan et al. (1999), based in all but one case on the ETFSI-Q (least-squares) model calculations. For the case of Th/Eu only, we have followed Cowan et al. (1999) and adopted an average value based on the ETFSI-Q, ETFSI-Q (least-squares) and finite range droplet with microscopic shell corrections (FRDM+HFB) models. Further discussion of the reliability of the various nuclear mass formulae along with new theoretical *r*-process calculations and new initial abundance ratios are presented in Burles et al. (2001).

In Table 4 we list the chronometer pair, the predicted (initial, zero-decay) abundances, the observed abundances, and the corresponding predicted age, based on a direct comparison between the predicted and observed ratios. We have not used the uncertain Os abundance to make these predictions, and we have deliberately grouped the uranium chronometers separately to emphasize that the weak uranium detection has much larger error bars associated with it than the thorium abundance does. Nevertheless, we have increased the number of chronometer pairs by a factor of 6 over most earlier studies, which only employed Th/Eu. (Cayrel et al. 2001 listed three pairs for their study of CS 31082-001, and Hannawald, Pfeiffer, & Kratz 2001 derived a new age estimate for CS 22892-052 from weighted averages of 15 Th/Ba-Ir pairs.) Our results demonstrate a general consistency between the various chronometer-pair estimates, with a mean value of 13.8 ± 4 Gyr. (We have also not employed the uncertain gold abundance for age estimates, but comparisons between predicted and observed Th/Au and U/Au suggest ages of 9.5 and 12.1 Gyr, respectively.) As an additional check on the age estimates, we have also included in Table 4 the solar system value for the different chronometer pairs. These solar *r*-process values are from B00 and are not dependent on nuclear mass models for the abundance ratios. The last column in the table lists age estimates based on comparing the solar ratios with the observed stellar ratios. These ages should be viewed as lower limits, since the solar values (at 4.5 Gyr old) are lower limits on the zero decay age *r*-process abundances. (Eu is stable, but Th has partially decayed.) There are some differences in the ages based on different chronometer pairs and between the theoretically predicted and solar values. We note, for example, that some of the predicted ages are less than the expected lower limit solar system age estimates. This is probably an indication that some of the predicted values from Cowan et al. (1999) need to be revised (see Burles et al. 2001). Nevertheless, the (lower limit) age derived from the solar abundance ratios, 13.2 Gyr, is not inconsistent with the average based on theoretical predicted *r*-process abundance ratios. Since the uranium detection is so weak, we could also consider our abundance measurement for this element as an upper limit rather than a detection. In this alternative the age estimates using this chronometer would more properly be lower limits. We have noted that possibility explicitly (by including greater than or equal signs) in Table 4 for the age estimates employing uranium.

Our derived age for BD +17°3248 (13.8 ± 4 Gyr) is in agreement with the cosmochronological ages for CS 31082-001 (12.5 ± 3 Gyr; Cayrel et al. 2001) and for CS 22892-052 and HD 115444 (15.6 ± 4 Gyr; Cowan et al. 1999; Westin et al. 2000). We caution, however, that all of these age estimates are very sensitive to uncertainties both in the theoretically predicted initial values and in the observations themselves; this is particularly true for our very weak detection of uranium. In addition, further investigation of any possible real offset between the rare earth elements and the third *r*-process peak elements and the corresponding effect on nucleocosmochronometry will be necessary. On the other hand, the overlap in age estimates found so far does seem promising, and we note that this technique has the advantage of being independent of (uncertain) models of Galactic chemical evolution.

5. CONCLUSIONS

We have gathered extensive ground-based (Keck and McDonald Observatory) and space-based (*HST*) high-resolution spectra of the metal-poor Galactic halo star BD

+17°3248. Our observations have detected the third *r*-process peak elements, Os, Ir, and Pt, making BD +17°3248 one of the few stars where these elements have been positively identified and the only star with detectable gold. In addition, we have tentatively detected uranium in this star, only the second such star that indicates the presence of this element. The detections of elements from Ge (using *HST*) up to U span the widest range (so far) in proton number of *n*-capture elements in halo stars.

The abundances of the heavy ($Z \geq 56$) *n*-capture elements in BD +17°3248 are consistent with a scaled solar system *r*-process abundance distribution. This result confirms earlier detailed abundance studies of UMP halo stars. Further, it suggests a robust nature for the *r*-process throughout the history of the Galaxy. However, the abundances of the lighter *n*-capture elements in the range $40 < Z < 56$ (i.e., Nb, Pd, and Ag) do not fall on the same curve as the heavier *n*-capture elements—a result that is consistent with the only other star with similar abundance information, CS 22892-052. This abundance pattern might be produced by two *r*-process sites (with one for the heavier and one for the lighter *n*-capture elements), perhaps from supernovae occurring at different frequencies, or neutron star binaries, or some combination of those. Alternatively, a single site with two regimes or sets of conditions in the same supernova site might also offer an explanation for the abundance pattern seen in this star.

We have employed the newly detected Th, U, and third *r*-process peak element abundances to make chronometric age estimates for BD +17°3248. The average of the various chronometric pairs suggests an age of 13.8 ± 4 Gyr for this star. This value is consistent, within error limits, with other chronometric age determinations for UMP and metal-poor Galactic halo stars. The still relatively large uncertainties reflect the sensitivity of the age estimate on both the predicted and observed abundance ratios. It is clear that additional stellar observations and theoretical studies, both already in progress, will be required to reduce the uncertainties so that this promising technique will be able to provide increasingly accurate age determinations of the oldest stars that will put limits on the age of the Galaxy and thus constrain cosmological age estimates.

We thank an anonymous referee for helpful comments to improve the paper. We thank Rica French for assistance with the data reduction and Jason Collier for assistance with the solar system abundances. This research has been supported in part by STScI grants GO-8111 and GO-08342, NSF grants AST 99-86974 (J. J. C.), AST 99-87162 (C. S.), AST 00-98508 and AST 00-98549 (T. C. B.), AST 98-19400 (J. E. L.), and PHY-9800980 (G. M. F.), and the ASCI/Alliances Center for Astrophysical Thermonuclear Flashes under DOE contract B341495 (J. W. T.). Support was also provided by the German BMBF (grant 06MZ9631).

APPENDIX

LINE DATA ADOPTED FOR THE ABUNDANCE ANALYSES

In this appendix we comment on the selection of atomic transition data for elements with $Z > 30$ and on the details of the line lists constructed for the synthetic spectrum computations. We discuss here only those elements for which CS 22892-052 abundances were given by Sneden et al. (2000a) without citation of atomic data sources and those for which different atomic data choices have been made than those already discussed in previous papers of this series. Thus, the reader is referred to S96 for a discussion of Sr I, Sr II, Y II, Zr II, Ba II, Sm II, Ho II, Er II, and Tm II, to Sneden et al. (1998) for some additional information on Os I, Pt I, and Pb I, and to Crawford et al. (1998) for Ag I. We also recomputed partition functions for most of the *n*-capture species studied here, instead of relying solely on those computed by Irwin (1981), which have become out of date for especially some ionized rare earth species.

Ge I, $Z = 32$.—The λ3039.07 line is the principal Ge abundance indicator, and it has been included in several laboratory analyses (see Sneden et al. 1998 for brief discussion and references). Here we adopt the *gf* from the recent study of Biémont et al. (1999), averaging their experimental and theoretical values. There are a few other Ge I lines that should be detectable on our *HST*/STIS spectrum of BD +17°3248, and we attempted to synthesize the ones at 2651.17 and 2651.57 Å as part of the modeling effort for the Pt I λ2650.85 line. Both of the lines proved, however, to suffer significant contamination from other atomic and OH features. In spite of these problems, it is possible to state that the profiles of these lines will not admit a large Ge abundance: we estimate that $\log \epsilon \lesssim 0.9$ from the λ2651.17 line and $\lesssim 0.6$ from the λ2650.85 line. These values generally support the abundance derived from the more trustworthy λ3039 line.

Nb II, $Z = 41$.—The *gf*-values are taken from Hannaford et al. (1985).

Pd I, $Z = 46$.—The *gf*-values are taken from Biémont et al. (1982).

La II, $Z = 57$.—A new laboratory study of this species by Lawler, Bonvallet, & Sneden (2001a) provides transition probabilities and hyperfine structure constants for a large number of lines. La II has a wide hyperfine pattern for many transitions, but La has just one naturally occurring isotope (^{139}La), so isotopic wavelength shifts are not needed. From these data we found 15 useful transitions in the BD +17°3248 spectrum, double the number employed by S96 for CS 22892-052. The old line lists were refined with the new data, and line lists for the new transitions were created according to the prescriptions given in the earlier paper.

Ce II, $Z = 58$.—We adopted the extensive set of new *gf*-values of Palmeri et al. (2000), who combined results from both experimental and theoretical investigations. We detected 22 lines of this species (compared with nine employed by S96 for the CS 22892-052 analysis). Since all Ce II lines are fairly weak in the BD +17°3248 spectrum, $\log(\mathrm{EW}/\lambda) \lesssim -5.3$, we were able to treat them as single lines without hyperfine or isotopic splitting.

Pr II, $Z = 59$.—This species has been reconsidered by Ivarsson, Litzén, & Wahlgren (2001), who have generated improved sets of energy levels, transition probabilities, and hyperfine structure constants for many lines. Since their data should be internally consistent, we limited our Pr abundance analysis to just those lines considered by Ivarsson et al. (2001), in preference to

the atomic data chosen by S96. As is the case for La, Pr has only one stable isotope (^{141}Pr). After identifying Pr II lines in the BD +17°3248 spectrum, we generated entirely new line lists for synthetic spectrum computations.

Nd II, $Z = 60$.—This species lacks a recent laboratory study. S96 attempted to reconcile the *gf* scales of Ward et al. (1985) and Maier & Whaling (1977), but the line-to-line scatter in *gf*-values between these two studies is large (Sneden et al. 2001b). Moreover, these laboratory studies only consider a small subset of the Nd II lines that can easily be observed in stellar spectra. Therefore, to produce *gf*-values for our lines, we simply averaged the large-sample, medium-accuracy *gf* results of Cowley & Corliss (1983) with those of Ward et al. (1985) and Maier & Whaling (1977) where available. This procedure allowed us to measure a large set of Nd II lines, but the resulting Nd abundance has a larger internal uncertainty ($\sigma = 0.17$) than most other rare earth elements.

Eu II, $Z = 63$.—New experimental *gf*-values and hyperfine/isotopic splitting constants have been determined by Lawler et al. (2001c), who also summarize the line data for this species from other relevant recent studies. Complete line parameters are now available for all strong Eu II transitions.

Gd II, $Z = 64$.—As in the S96 study, we employed the *gf*-values of Bergström et al. (1988) that were derived directly from their lifetime measurements. For other lines, we adopted the values of Corliss & Bozman (1962), multiplied by 1.3 as recommended by Bergström et al. (1988). The proposed renormalization of the older *gf* scale really only applies to transitions connecting to those levels for which Bergström et al. (1988) measured lifetimes. However, derivation of Gd abundances using only the six measured lines in BD +17°3248 in common with the Bergström et al. (1988) study yielded nearly the same mean abundance as computed from the whole set of 15 lines, and the sample standard deviations σ were identical. Therefore, all Gd II lines were given equal weight in the abundance analysis.

Tb II, $Z = 65$.—Poorly determined transition parameters and intrinsic weakness of all lines of this species in the Sun and metal-poor stars in the past have led to very uncertain abundances of Tb. New laboratory *gf* and hyperfine structure data (^{159}Tb is the only stable isotope of this element, so isotopic wavelength shifts are not needed) have been obtained by Lawler et al. (2001b) for Tb II. These data, along with updated partition functions, have been used to analyze the five Tb II lines that could be cleanly detected in the BD +17°3248 spectrum. These lines yield very consistent Tb abundances in this star.

Dy II, $Z = 66$.—There are several laboratory analyses of this species, and for maximum internal consistency we adopted only the *gf*-values from the recent study of Wickliffe, Lawler, & Nave (2000). However, use of the Kusz (1992) or Biémont & Lowe (1993) *gf*-values would not materially alter the Dy abundance derived for BD +17°3248, since all three laboratory studies find similar results for the stronger lines of Dy II.

Os I, $Z = 76$.—The *gf*-values have been taken from Kwiatkowski et al. (1984) or scaled from those of Corliss & Bozman (1962) according to the lifetime measurements of Kwiatkowski et al. (1984). The resulting abundances derived from five lines (two from Keck/HIRES and three from *HST*/STIS spectra) are in excellent internal agreement. However, all Os I lines are weak in BD +17°3248. Moreover, the $\lambda\lambda$2838.63 and 3301.57 features are particularly blended with other atomic lines, and the S/N of the Keck/HIRES spectrum in the region of the λ3267.95 line is not high; the reader should exercise caution in interpretation of the Os abundance.

Ir I, $Z = 77$.—The *gf*-values are based on the lifetime measurements of Gough, Hannaford, & Lowe (1983).

Pt I, $Z = 78$.—Using *HST*/GHRS spectra of a few very small wavelength intervals, Sneden et al. (1998) synthesized the Pt I $\lambda\lambda$2929.79, 3064.71 lines to derive abundances of Pt in the *r*-process–rich star HD 115444 and in the higher metallicity giant HD 126538 ([Fe/H] = −1.65, [*n*-capture/Fe] ∼ 0). The λ3064 line is not easy to work with as it is nearly buried in a thicket of other atomic and OH molecular contaminants. The much larger wavelength range of the STIS spectrum allowed detection of five Pt I lines in BD +17°3248, including the very strong one at 2659.45 Å. We employed the *gf*-values recommended by Morton (2000), based on experimental results of Gough, Hannaford, & Lowe (1982), Lotrian & Guern (1982), and Reader et al. (1990).

Au I, $Z = 79$.—The derived Au abundance should be interpreted with care. This abundance is determined from the two resonance lines at 2427.94 and 2675.94 Å, whose *gf*-values are well determined (Hannaford, Larkins, & Lowe 1981; Gaarde et al. 1994). These lines were clearly detected in the spectrum of BD +17°3248, but both suffer substantial blending problems. Discussion of the λ2675 line was given in § 3.3. Derivation of an Au abundance from the λ2427.94 line is more problematic because it sits on the side of a very strong Fe I line at 2428.06 Å, and only a very rough guesstimate of $\log \epsilon(\mathrm{Au}) \sim -0.2$ could be made, with an uncertainty of at least ±0.5 dex.

U II, $Z = 92$.—The *gf* of the λ3859.57 line was taken from the new study by Lundberg et al. (2001).

REFERENCES

Alonso, A., Arribas, S., & Martinez-Roger, C. 1998, A&AS, 131, 209
———. 1999, A&AS, 140, 261
———. 2001, A&A, 376, 1039
Anthony-Twarog, B. J., & Twarog, B. A. 1994, AJ, 107, 1577
———. 1998, AJ, 116, 1922
Aoki, W., et al. 2001, ApJ, 561, 346
Arlandini, C., Käppeler, F., Wisshak, K., Gallino, R., Lugaro, M., Busso, M., & Staniero, O. 1999, ApJ, 525, 886
Balachandran, S., & Carney, B. W. 1996, AJ, 111, 946
Barlow, T. A., & Sargent, W. L. W. 1997, AJ, 113, 136
Beers, T. C., Preston, G. W., & Shectman, S. A. 1985, AJ, 90, 2089
———. 1992, AJ, 103, 1987
Beers, T. C., Rossi, S., Norris, J. E., Ryan, S. G., & Shefler, T. 1999, AJ, 117, 981
Beers, T. C., & Sommer-Larsen, J. 1995, ApJS, 96, 175
Bell, R. A., & Gustafsson, B. 1978, A&AS, 34, 229
Bergström, H., Biemont, E., Lundberg, H., & Persson, A. 1988, A&A, 192, 335
Biémont, E., Grevesse, N., Kwiatkowski, M., & Zimmermann, P. 1982, A&A, 108, 127
Biémont, E., & Lowe, R. M. 1993, A&A, 273, 665
Biémont, E., Lyngå, C., Li, Z. S., Svanberg, S., Garnir, H. P., & Doidge, P. S. 1999, MNRAS, 303, 721
Boesgaard, A. M., King, J. R., Deliyannis, C. P., & Vogt, S. S. 1999, AJ, 117, 492
Bond, H. E. 1980, ApJS, 44, 517
Burles, S., Truran, J. W., Cowan, J. J., Sneden, C., Kratz, K.-L, & Pfeiffer, B. 2001, preprint
Burris, D. L., Pilachowski, C. A., Armandroff, T. A., Sneden, C., Cowan, J. J., & Roe, H. 2000, ApJ, 544, 302 (B00)

Cameron, A. G. W. 2001, ApJ, 562, 456
Carbon, D., Langer, G., Butler, D., Kraft, R., Suntzeff, N., Kemper, E., Trefzger, C., & Romanishin, W. 1982, ApJS, 49, 207
Carney, B. W. 1983, AJ, 88, 610
Cayrel, R. 1996, A&A Rev., 7, 217
Cayrel, R., et al. 2001, Nature, 409, 691
Clariá, J. J., Minniti, D., Piatti, A. E., & Lapasset, E. 1994, MNRAS, 268, 733
Corliss, C. H., & Bozman, W. R. 1962, Experimental Transition Probabilities for Spectral Lines of Seventy Elements, NBS Monograph 32 (Washington, DC: US Govt. Printing Office)
Cowan, J. J., Burris, D. L., Sneden, C., McWilliam, A., & Preston, G. W. 1995, ApJ, 439, L51
Cowan, J. J., McWilliam, A., Sneden, C., & Burris, D. L. 1997, ApJ, 480, 246
Cowan, J. J., Pfeiffer, B., Kratz, K.-L., Thielemann, F.-K., Sneden, C., Burles, S., Tytler, D., & Beers, T. C. 1999, ApJ, 521, 194
Cowan, J. J., Sneden, C., & Truran, J. W. 2001, in Proceedings of the 20th Texas Symposium on Relativistic Astrophysics, ed. C. Wheeler & H. Martel, (New York: AIP), 337
Cowan, J. J., Sneden, C., Truran, J. W., & Burris, D. L. 1996, ApJ, 460, L115
Cowley, C. R., & Corliss, C. H. 1983, MNRAS, 203, 651
Crawford, J. L., Sneden, C., King, J. R., Boesgaard, A. M., & Deliyannis, C. P. 1998, AJ, 116, 2489
Dupree, A. K., & Smith, D. H. 1995, AJ, 110, 405
Edvardsson, B., Andersen, J., Gustafsson, B., Lambert, D. L., Nissen, P. E., & Tomkin, J. 1993, A&A, 275, 101
Fitzpatrick, M. J., & Sneden, C. 1987, BAAS, 19, 1129
François, P., Spite, M., & Spite, F. 1993, A&A, 274, 821
Gaarde, M. B., Zerne, R., Caiyan, L., Zhankui, J., Larsson, J., & Svanberg, S. 1994, Phys. Rev. A, 50, 209
Gilliland, R. L., Morris, S. L., Weymann, R. J., Ebbets, D. C., & Linder, D. J. 1992, PASP, 104, 367
Gough, D. S., Hannaford, P., & Lowe, R. M. 1982, J. Phys. B, 15, L431
———. 1983, J. Phys. B, 16, 785
Gratton, R., & Sneden, C. 1991, A&A, 241, 501
———. 1994, A&A, 287, 927
Gratton, R. G., Sneden, C., Carretta, E., & Bragaglia, A. 2000, A&A, 354, 169
Grevesse, N., & Sauval, A. J. 1998, Space Sci. Rev., 85, 161
Hannaford, P., Larkins, P. L., & Lowe, R. M. 1981, J. Phys. B, 14, 2321
Hannaford, P., Lowe, R. M., Biémont, E., & Grevesse, N. 1985, A&A, 143, 447
Hannawald, M., Pfeiffer, B., & Kratz, K.-L. 2001, in ASP Conf. Ser. 245, Astrophysical Ages and Time Scales, ed. T. von Hippel, N. Manset, & C. Simpson (San Francisco: ASP), 310
Hartkopf, W. I., & Yoss, K. M. 1982, AJ, 87, 1679
Holweger, H., & Müller, E. A. 1974, Sol. Phys., 39, 19
Irwin, A. W. 1981, ApJS, 45, 621
Israelian, G., García Lopez, R. J., & Rebolo, R. 1998, ApJ, 507, 805
Ivarsson, S., Litzén, U., & Wahlgren, G. M. 2001, Phys. Scr., in press
Johnson, J. A., & Bolte, M. 2001, ApJ, 554, 888
Käppeler, F., Beer, H., & Wisshak, K. 1989, Rep. Prog. Phys., 52, 945
Klochkova, V. G., Ermakov, S. V., & Panchuk, V. E. 1999, Ap&SS, 265, 185
Kraft, R. P., Suntzeff, N. B., Langer, G. E., Trefzger, C. F., Friel, E., Stone, R. P., & Carbon, D. F. 1982, PASP, 94, 55
Krishnaswamy-Gilroy, K., Sneden, C., Pilachowski, C. A., & Cowan, J. J. 1988, ApJ, 327, 298
Kurucz, R. L. 1995, in ASP Conf. Ser. 81, Workshop on Laboratory and Astronomical High Resolution Spectra, ed. A. J. Sauval, R. Blomme, & N. Grevesse (San Francisco: ASP), 583
Kurucz, R. L., Furenlid, I., Brault, J., & Testerman, L. 1984, Solar Flux Atlas from 296 to 1300 nm (Cambridge: Harvard Univ. Press)
Kusz, J. 1992, A&AS, 92, 517
Kwiatkowski, M., Zimmermann, P., Biémont, E., & Grevesse, N. 1984, A&A, 135, 59
Lawler, J. E., Bonvallet, G., & Sneden, C. 2001a, ApJ, 556, 452
Lawler, J. E., Wickliffe, M. E., Cowley, C. R., & Sneden, C. 2001b, ApJS, 137, 341
Lawler, J. E., Wickliffe, M. E., Den Hartog, E. A., & Sneden, C. 2001c, ApJ, 563, 1075
Lotrian, J., & Guern, Y. 1982, J. Phys. B, 15, 69
Luck, R. E., & Bond, H. E. 1981, ApJ, 244, 919
Lundberg, H., Johansson, S., Nilsson, H., & Zhang, Z. 2001, A&A, 372, L50
Maier, R. S., & Whaling, W. 1977, J. Quant. Spectrosc. Radiat. Transfer, 18, 501
Mathews, G. J., Bazan, G., & Cowan, J. J. 1992, ApJ, 391, 719
McWilliam, A. 1998, AJ, 115, 1640
McWilliam, A., Preston, G. W., Sneden, C., & Searle, L. 1995a, AJ, 109, 2757
McWilliam, A., Preston, G. W., Sneden, C., & Shectman, S. 1995b, AJ, 109, 2736
Meléndez, J., Barbuy, B., & Spite, F. 2001, NewA Rev., 45, 551
Moore, C. E., Minnaert, M. G. J., & Houtgast, J. 1966, The Solar Spectrum 2935 A to 8770 A, NBS Monograph 61 (Washington, DC: US Govt. Printing Office)
Morell, O., Källander, D., & Butcher, H. R. 1992, A&A, 259, 543
Morton, D. C. 2000, ApJS, 130, 403
Norris, J. E., Ryan, S. G., & Beers, T. C. 1997, ApJ, 489, L169
Palmeri, P., Quinet, P., Wyart, J.-F., & Biémont, E. 2000, Phys. Scr., 61, 323
Perryman, M. A. C., et al. 1997, A&A, 323, L49
Pfeiffer, B., Kratz, K.-L., & Thielemann, F.-K. 1997, Z. Phys. A, 357, 235
Pfeiffer, B., Kratz, K.-L., Thielemann, F.-K., & Walters, W. B. 2001a, Nucl. Phys. A, 693, 282
Pfeiffer, B., Ott, U., & Kratz, K.-L. 2001b, Nucl. Phys. A, 688, 575
Pilachowski, C. A., & Sneden, C. 1999, AAS, 195, 5006
Pilachowski, C. A., Sneden, C., & Booth, J. 1993, ApJ, 407, 699
Pilachowski, C. A., Sneden, C., & Kraft, R. P. 1996, AJ, 111, 1689
Raiteri, C. M., Gallino, R., Busso, M., Neuberger, D., & Käppeler, F. 1993, ApJ, 419, 207
Reader, J., Acquistra, N., Sansonetti, C. J., & Sansonetti, J. E. 1990, ApJS, 72, 831
Rosswog, S., Liebendorfer, M., Thielemann, F.-K., Davies, M. B., Benz, W., & Piran, T. 1999, A&A, 341, 499
Ryan, S. G., Norris, J. E., & Beers, T. C. 1996, ApJ, 471, 254
Smith, G. H., & Dupree, A. K. 1988, AJ, 95, 1547
Sneden, C. 1973, ApJ, 184, 839
Sneden, C., Cowan, J. J., Burris, D. L., & Truran, J. W. 1998, ApJ, 496, 235
Sneden, C., Cowan, J. J., Ivans, I. I., Fuller, G. M., Burles, S., Beers, T. C., & Lawler, J. E. 2000a, ApJ, 533, L139
Sneden, C., Cowan, J. J., Lawler, J. E., Burles, S., Beers, T. C., & Fuller, G. M. 2002, ApJ, 566, L25
Sneden, C., Cowan, J. J., & Truran, J. W. 2001a, in Cosmic Evolution, ed. E. Vangioni-Flam, R. Ferlet, & M. Lemoine (Singapore: World Scientific), 179
Sneden, C., Gratton, R. G., & Crocker, D. A. 1991a, A&A, 246, 354
Sneden, C., Johnson, J., Kraft, R. P., Smith, G. H., Cowan, J. J., & Bolte, M. S. 2000b, ApJ, 536, L85
Sneden, C., Kraft, R. P., Prosser, C. F., & Langer, G. E. 1991b, AJ, 102, 2001
Sneden, C., Kraft, R. P., Shetrone, M. D., Smith, G. H., Langer, G. E., & Prosser, C. F. 1997, AJ, 114, 1964
Sneden, C., Lawler, J. E., & Cowan, J. J. 2001b, Phys. Scr., in press
Sneden, C., McWilliam, A., Preston, G. W., Cowan, J. J., Burris, D. L., & Armosky, B. J. 1996, ApJ, 467, 819 (S96)
Sneden, C., & Parthasarathy, M. 1983, ApJ, 267, 757
Sneden, C., & Pilachowski, C. A. 1985, ApJ, 288, L55
Sneden, C., Pilachowski, C. A., & Kraft, R. P. 2000c, AJ, 120, 1351
Sneden, C., Preston, G. W., McWilliam, A., & Searle, L. 1994, ApJ, 431, L27
Spite, M., & Spite, F. 1978, A&A, 67, 23
Toenjes, R., Schatz, H., Kratz, K.-L., Pfeiffer, B., Beers, T. C., Cayrel, R., Cowan, J. J., & Hill, V. 2001, in ASP Conf. Ser. 245, Astrophysical Ages and Time Scales, ed. T. von Hippel, N. Manset, & C. Simpson (San Francisco: ASP), 376
Truran, J. W. 1981, A&A, 97, 391
Tull, R. G., MacQueen, P. J., Sneden, C., & Lambert, D. L. 1995, PASP, 107, 251
Vogt, S. S., et al. 1994, Proc. SPIE, 2198, 362
Ward, L., Vogel, O., Arnesan, A., Hallin, R., & Wännström, A. 1985, Phys. Scr., 31, 161
Wasserburg, G. J., Busso, M., & Gallino, R. 1996, ApJ, 466, L109
Wasserburg, G. J., & Qian, Y.-Z. 2000, ApJ, 529, L21
Westin, J., Sneden, C., Gustafsson, B., & Cowan, J. J. 2000, ApJ, 530, 783
Wheeler, C., Cowan, J. J., & Hillebrandt, W. 1998, ApJ, 493, L101
Wheeler, C., Sneden, C., & Truran, J. W. 1989, ARA&A, 27, 279
Wickliffe, M. E., Lawler, J. E., & Nave, G. 2000, J. Quant. Spectrosc. Radiat. Transfer, 66, 363
Wisshak, K., Voss, F., & Käppeler, F. 1996, in Proceedings of the 8th Workshop on Nuclear Astrophysics, ed. W. Hillebrandt & E. Müller (Munich: MPI), 16
Woolf, V. M., Tomkin, J., & Lambert D. L. 1995, ApJ, 453, 660